SIMULTANEOUS ADSORPTION AND DEGRADATION OF METHYLENE BLUE USING MAGNETIC CARBON NANOTUBES

LEE EE CHIA

A project report submitted in partial fulfilment of the requirements for the award of Bachelor of Engineering (Honours) Mechanical Engineering

**Lee Kong Chian Faculty of Engineering and Science
Universiti Tunku Abdul Rahman**

April 2020

DECLARATION

I hereby declare that this project report is based on my original work except for citations and quotations which have been duly acknowledged. I also declare that it has not been previously and concurrently submitted for any other degree or award at UTAR or other institutions.

Signature   :

Name   :   Lee Ee Chia

ID No.   :   15UEB05305

Date   :   23/04/2020

APPROVAL FOR SUBMISSION

I certify that this project report entitled **"SIMULTANEOUS ADSORPTION AND DEGRADATION OF METHYLENE BLUE USING MAGNETIC CARBON NANOTUBES"** was prepared by **LEE EE CHIA** has met the required standard for submission in partial fulfilment of the requirements for the award of Bachelor of Engineering (Honours) Chemical Engineering at Universiti Tunku Abdul Rahman.

Approved by,

Signature	:	
Supervisor	:	Ts. Dr. Shuit Siew Hoong
Date	:	23/04/2020

Signature	:	
Co-Supervisor	:	Ts. Dr. Tee Shiau Foon
Date	:	23/04/2020

ACKNOWLEDGEMENTS

I would like to thank everyone who had contributed to the successful completion of this project. I would like to express my gratitude to my research supervisor, Dr. Shuit Siew Hoong for his invaluable advice, guidance and his enormous patience throughout the development of the research.

In addition, I would also like to express my gratitude to my loving parents and friends who had helped and given me encouragement in completing this report. Without them, I would have not resolved my problems which I had faced during my research work and report writing.

ABSTRACT

Magnetic multiwalled carbon nanotubes (MWCNTs-Fe_3O_4 nanocomposites) synthesized by solvent free direct doping method, was subjected for the removal of cationic methylene blue (MB) dyes. The functional groups, phase structure, surface morphology, surface area and thermal stability of the synthesized nanocomposites were then characterized by various physicochemical characterizations such as Fourier transform infrared (FTIR), X-ray powder diffraction (XRD), scanning electron microscopy coupled with energy dispersive X-ray (SEM-EDX), Braunauer-Emmett-Teller (BET) and thermogravimetric analysis (TGA). FTIR analysis confirmed the presence of carboxylic groups in the acid treated MWCNTs as well as the successfully doping of Fe_3O_4 nanoparticles onto MWCNTs. Next, XRD and SEM-EDX analysis further supported that the synthesized nanocomposites consisted of both hexagonal graphite structure of MWCNTs and the inverse spinel structure of Fe_3O_4 nanoparticles. In addition, BET analysis indicated that the surface area of the synthesized MWCNTs-Fe_3O_4 nanocomposites increased significantly as compared to the raw and acid treated MWCNTs. TGA analysis also showed that the MWCNTs-Fe_3O_4 nanocomposites to possess high thermal stability. Design Expert simulation was employed to determine the effects of various process parameters in the adsorption and degradation of MB. The process parameters studied included pH (2 – 10), initial MB concentration (10 – 50 mg/L), MWCNTs-Fe_3O_4 nanocomposites dosage (10 – 30 mg) and H_2O_2 concentration (5 – 20 mmol/L). The optimum reaction condition was then acquired via the response surface methodology (RSM) associated with central composite design (CCD). Results showed that an average optimum percentage of MB degradation of 95.92 % can be achieved under the following reaction conditions: pH of 5.86, initial MB concentration of 32.22 mg/L, MWCNTs-Fe_3O_4 nanocomposites dosage of 27 mg and H_2O_2 concentration of 13.02 mmol/L.

TABLE OF CONTENTS

LIST OF TABLES

LIST OF FIGURES

LIST OF SYMBOLS / ABBREVIATIONS

CNTs	carbon nanotubes
COD	chemical oxygen demand
DNA	deoxyribonucleic acid
MB	methylene blue
MWCNTs	multiwalled carbon nanotubes
RNA	ribonucleic acid
SEM	scanning electron microscope
SWCNTs	single walled carbon nanotubes
UV-Vis	ultraviolet-visible
FTIR	Fourier transform infrared
XRD	x-ray powder diffraction
SEM	scanning electron microscopy
EDX	energy dispersive X-ray
BET	Braunauer-Emmett-Teller
TGA	thermogravimetric analysis
DOE	design of experiment
-COOH	carboxylic acid
FCC	face-centred cubic
Fe^{2+}	ferrous ion
Fe^{3+}	ferric ion
$FeCl_2$	iron (II) chloride
$FeCl_3.6H_2O$	iron (III) chloride hexahydrate
Fe_3O_4	iron oxide
$FeSO_4 \cdot 7H_2O$	ferrous sulphate heptahydrate
HCl	hydrochloric acid
HNO_3	nitric acid
H_2O_2	hydrogen peroxide
KBr	potassium bromide
NaOH	sodium hydroxide
$\cdot OH$	hydroxyl radical

•OOH	hydroperoxyl radical
SDS	sodium dodecyl sulphate
°C	degree Celsius
cm^{-1}	per centimetre
nm	nanometre
M	molarity
mg	milligram
mg/L	milligram per litre
min	minute
mL	millilitre
mmol	millimole
mmol/L	millimole per litre
G	gauss
g	gram
g/L	gram per litre
h	hour
s^{-1}	per second
°	degree
%	percent

LIST OF APPENDICES

CHAPTER 1

INTRODUCTION

1.1 General Introduction

Water is vital for all living things because it involved in daily activities related to industrial, agricultural and domestic cares, which include washing, bathing, cleaning, cooking and drinking (Haseena, et al., 2017; Sharma, et al., 2018). Hence, water quality affects various aspects of human life such as food, energy, economic and health. Even though water can be renewed on its own by sedimentation, this process takes time and is unproductive when large number of hazardous contaminants available in water. Nowadays, the reduction supply of clean water sources becomes one of the major public concerns as the population on the earth is increasing. The growing demands of manufacture products caused more industrialization and thus causing more utilization of water for industrial processes (Jasrotia, 2015). High usage and discharge of untreated water further lead to water pollution, which is currently a severe problem as it has not only possessed negative impact to environment but also to human health.

Water pollution occurs when the poor-treated or untreated wastes that containing dangerous components entering the water bodies either by direct or indirect discharge. It originated from two broad categories of sources, which were non-point sources and point sources. The pollution that happened over a wide area that was difficult to localized was classified under non-point sources. For instance, flow of fertilizer and pesticides which run off from lawns and farms into streams. Conversely, if pollution induced by drain or piping system from a single and localized source of pollution, it was categorized as point sources pollution. Point sources pollution included domestic sewage and industrial wastes like heavy metal ions and dyes (EPA Victoria, 2018; Water Education Foundation, n.d.). Dyes were widely employed in leather, textile, rubber, cosmetics, paper and synthetic detergent industries. According to Carmen and Daniela, (2012), dyes were built-up by complex aromatic molecule with synthetic origin which make them greatly resist to biodegradation by conventional biological and physical oxidation treatment processes. The dyes in

water are highly visible even with the concentration of less than 1 mg/L and the water that containing dyes is unsafe to be consumed.

Textile industry is the largest producer of dye effluents. The World Bank approximated that about 20 % of the industrial water contamination was due to the dyeing of textiles. Kant (2012) reported that the textile industry produced more than 3600 dyes yearly and the textile industry was the second topmost producer of wastewater after agricultural. Textile wastewater was commonly characterized by high content of salts, dyestuff, alkalinity, high chemical oxygen demand (COD) derived from additives, heat, acidity, color, suspended solid and fluctuating pH. The primary environment concern of textile wastewater was the dissolved organic dye compounds due to the carcinogenic and aromatics properties of these chemical compounds (Jasrotia, 2015).

Normally, dyes were grouped into anionic, cationic and non-ionic dyes. There were variety dyes including malachite green, Congo red, methylene blue (MB), methyl orange and toluidine blue. MB is a cationic, organic dye with water-soluble properties that mostly adopted as dyeing material for silk, wood and cotton (Selen, et al., 2015; Eljiedi and Kamari, 2017). Excessive levels of MB can result in eye burns, nausea, profuse sweating, vomiting, diarrhoea, as well as mental confusion and breathlessness (Chunha, 2016; Fayazi, et al., 2016). A variety of chemical, physical and biological technologies had been used to remove MB from the wastewater, for example coagulation-flocculation, photodecomposition, chemical precipitation, adsorption, biosorption and electrochemical treatment. Among the above methods, adsorption was broadly employed due to its simplicity and comparatively low cost in operation (Hassan, Abdel-Mohsen and Fouda, 2014).

Various adsorbents such as activated carbon, zeolite, carbon nanotubes (CNTs) and clay were employed for the removal of MB. Other than that, some agricultural wastes include orange peel, rice straw and pine cone were also considered as the potential adsorbents for MB removal. Among the mentioned adsorbents, CNTs appeared to be an interesting alternative to serve as the adsorbent for the removal of MB owing to their unique electronic and geometry, chemical, thermal and mechanical properties (Song, et al., 2011; Tae and Tannenbaum, 2011). CNTs are commonly defined as "rolled-up" sheets of graphite. They can present as a rolled graphite sheet named as single walled

carbon nanotubes (SWCNTs) or exists as multiple concentric tubes that fitted one inside the other which were known as multiwalled carbon nanotubes (MWCNTs) (Sljukic, Banks and Compton, 2006). Between SWCNTs and MWCNTs, the latter are more favourable due to its lower price and excellent properties for the adsorption process.

Nevertheless, MWCNTs were inconvenience in practical applications as they were difficult to be collected from the dispersing media. Therefore, iron oxide nanoparticles (Fe_3O_4) were introduced onto the surface of MWCNTs to create magnetic MWCNTs (MWCNTs-Fe_3O_4 nanocomposites), which can be simply removed by an external magnetic field (Huang, Yu and Jiang, 2014). Yet, exhausted MWCNTs-Fe_3O_4 nanocomposites were required to be regenerated for further use. During regeneration process, separation of MB from MWCNTs-Fe_3O_4 nanocomposites will indirectly create secondary wastes. Thus, Fenton degradation process coupled with the adsorption process was used to overcome this problem. Besides providing magnetic properties during separation process, Fe_3O_4 nanoparticles also acted as a catalyst for Fenton degradation process. Fe_3O_4 nanoparticles reacted with hydrogen peroxide (H_2O_2) to produce high oxidizing hydroxyl radicals ($^\bullet OH$) (Pena, et al., 2012). The $^\bullet OH$ radicals with high oxidizing ability can immediately attack MB, leading to the degradation and mineralization of MB.

There were numerous Fenton degradation processes, for instance homogeneous Fenton reaction, heterogeneous Fenton-like reaction and photo-Fenton reaction. Among them, heterogeneous Fenton-like reaction was more favourable because it can take place at a neutral pH, leaving aside the requirement for the neutralization and acidification process, hence preventing the formation of sludge. Besides, the catalysts also have the ability to be regenerated and recycled. In addition, heterogeneous catalysts were easy to be handled, thereby simplify the waste treatment processes (Pereira, Oliveira and Murad, 2012).

1.2   Problem Statement

As reported by Almaamary, et al. (2017), as well as Abu-El-Halawa, Zabin and Abu-Sittah (2016), most of the conventional methods used to remove MB were not practicable on large scale which involved high capital and operational costs.

Although biological treatment was considered as the most economical alternative, it required large area for the construction of digestion pond. Besides, biological treatment was not suitable in treating MB because of its low biodegradation and bio-efficacy (Karthik, et al., 2015). Among the possible MB removal techniques, adsorption was considered the most versatile and widely used technique in many industries in terms of its effectiveness, efficiency and economy. On top of that, the advantages of adsorption process included low operation cost, no sludge formation, ease of operation and simple in design (Eljiedi and Kamari, 2017). Furthermore, it did not require large area of land which can significantly cut down the investment cost (Rashed, 2013).

The regeneration issue has prohibited activated carbon to be a broadly used adsorbent for MB removal. In addition, other common adsorbents such as clay, zeolite, rice husk, fruit peels and so on encountered low adsorption capacity. With the advancement of nanotechnology in recent years, MWCNTs become a more attractive way to remove MB from wastewater due to their relatively large surface area per unit volume, favourable physiochemical and thermal stability. Moreover, their hollow and layered structures contribute to higher sorption capacity as compared to other adsorbents (Yao, et al., 2011; Prola, et al., 2013; Long and Yang, 2001; Rajabi, Mahanpoor and Moradi, 2017).

Apart from that, conventional adsorption process required additional separation process to remove the spent adsorbent before discharging the water. Moreover, nanoparticles such as MWCNTs were inconvenience to be applied practically because of their poor solubility and difficulty to collect them from the dispersing media by tedious centrifugation process (Fugetsu, et al., 2004; Malayeri, Sohrabi and Ghourchian, 2012). To solve the problems, MWCNTs-Fe_3O_4 nanocomposites that can be wholly dispersed in the medium were employed as they can be easily removed from the aqueous media by external magnet. Therefore, they were capable in treating huge amount of wastewater within a short period.

However, Fayazi, et al. (2016) stated that adsorption utilized by MWCNTs-Fe_3O_4 nanocomposites will not destroy the pollutants, but was simply transferring them to another kind of wastes. This meant that during regeneration of exhausted MWCNTs-Fe_3O_4 nanocomposites, MB that was separated out will become secondary waste and cause disposal problem. To

overcome this problem, heterogeneous Fenton-like degradation was employed to completely degrade and mineralize MB from the medium. This method had its own unique dominance, for instance simple operation, high degradation efficiency, mild reaction conditions, inexpensive materials and environmentally friendly (Hu, et al., 2011).

1.3   Aim and Objectives

The main goal in this study is to synthesis magnetic MWCNTs from pristine MWCNTs and use it to adsorb and degrade MB. Specific objectives for this study include:

    i.   To synthesis and characterize the magnetic MWCNTs.

    ii.   To investigate the effect of parameters for the adsorption of MB.

    iii.   To study the effect of parameters for the degradation of MB via Fenton reaction.

1.4   Scope of the Study

One of the goals for this study is to synthesis and characterize the magnetic MWCNTs. A solvent-free method, also known as direct doping, was used to synthesis the magnetic MWCNTs with a ratio of 1.5:1 for both pristine MWCNTs and Fe_3O_4 nanoparticles. Then, the magnetic MWCNTs was characterized by Fourier transform infrared (FTIR) and X-ray powder diffraction (XRD) in order to determine their functional group and phase structure. Moreover, scanning electron microscopy coupled with energy dispersive X-ray (SEM-EDX) was also used to characterize the magnetic MWCNTs to determine their surface morphology. Besides, the specific surface area of the magnetic MWCNTs was determined by using Brunauer-Emmett-Teller (BET), and lastly thermogravimetric analysis (TGA) was utilized to study the thermal stability of the magnetic MWCNTs.

Next, the synthesized magnetic MWCNTs was used to study the adsorption of MB. There were several parameters that affected the adsorption efficiency of MB by using magnetic MWCNTs. In this study, three parameters were identified such as pH in a range of 2 to 10, initial MB concentration between 10 and 50 mg/L and the adsorbent dosage range from 10 to 30 mg.

Lastly, the effect of parameters for the degradation of MB via Fenton degradation was be investigated. There were total four parameters to be considered, which include pH, initial MB concentration, MWCNTs-Fe$_3$O$_4$ nanocomposites dosage and H$_2$O$_2$ concentration. The pH, initial MB concentration and the MWCNTs-Fe$_3$O$_4$ nanocomposites dosage were elucidated in the same range as the above while for the H$_2$O$_2$ concentration, it ranged between 5 to 20 mmol/L.

1.5 Outline of the Report

This report included five chapters, which were introduction, literature review, methodology, results and discussion, as well as conclusion and recommendation.

Chapter 1 introduced the general outline on the causes and effects of the water pollution, together with the types of water pollution and the techniques to treat the water pollution. Besides, it also comprised the problem statement that stated the problem faced by the current adsorbent and adsorption process. Lastly, it also consisted of the aims, objectives and scope of this study to overcome the problem encountered. Chapter 2 was the literature review. In this chapter, the brief background of MB, CNTs, Fe$_3$O$_4$ nanoparticles, magnetic MWCNTs and Design Expert simulation were covered. Furthermore, it also described the mechanism of adsorption, degradation of MB by the magnetic MWCNTs. Moreover, the characterization equipment such as FTIR, XRD, SEM-EDX, BET and TGA were introduced.

Chapter 3 introduced the materials and apparatus that used in this study. Next, it also presented the methodology to synthesize the magnetic MWCNTs and the steps to characterize the synthesized catalysts by employing FTIR, XRD, SEM-EDX, BET and TGA, as well as the method of determining the effect of different process parameters (pH, initial MB concentration, MWCNTs-Fe$_3$O$_4$ nanocomposites dosage and H$_2$O$_2$ concentration) on the percentage of adsorption and degradation of MB via Design Expert simulation.

Chapter 4 explained the results obtained from the characterization and Design Expert simulation by comparing the results gained with the results reported by other authors in the literature review. Lastly, Chapter 5 concluded the results in this study and listed down the recommendations required to improve the future research work.

CHAPTER 2

LITERATURE REVIEW

2.1   Methylene Blue

MB was primarily manufactured as a basic aniline dye for textile industry in 1876 (Berneth, 2008). It is a chemical compound that having a heterocyclic aromatic ring with a molecular formula of $C_{16}H_{18}N_3ClS$. It can be applied in numerous industries such as chemistry and biology. At room temperature, it appears as a dark green solid powder with inodorous properties. In water, it dissolves and produces a solution with blue color. Figure 2.1 below depicted the chemical structure of MB while its properties were summarised in Table 2.1.
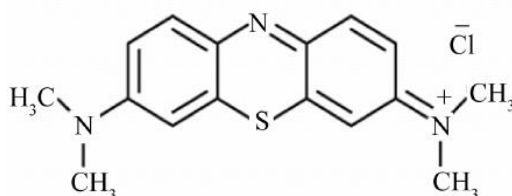
Figure 2.1: Chemical Structure of MB (Elmorsi, 2011).

Table 2.1: Properties of MB (Al-Qodah, et al., 2007).

Chemical formula	$C_{16}H_{18}N_3ClS$
Molecular mass (g/mol)	319.85
pH	Basic
Color	Dark green powder that yields a blue solution when dissolved in water
Odor	Odorless
Physical state at 25℃	Solid
Solubility	3.55 %

2.1.1   Applications and Hazards

In analytical chemistry, the oxidizable MB was usually employed as a redox indicator to detect oxidising agents. During the detection, the solution will appear as blue color when the electrons were removed from the MB, which

signified a chemical change. It was also used as a photosensitizer to produce singlet oxygen when exposed to both light and oxygen. Besides, it was widely used as dyes in textile industry. According to Dawood and Sen (2014), the global consumption of dye in textile industry went beyond 10 000 tons per annum and around 10 to 15 % of these dyes were discharged to the environment during the dyeing process.

MB can be applied in biology field as dye for numerous staining procedures, including Jenner's stain and Wright's stain to stain tissues samples and detect nucleic acids. MB can be utilized in the inspection of DNA or RNA under the microscope or in a gel since it is a temporary staining method. In medicine, it was employed to treat different illnesses and disorders, such as herpes infections, methemoglobinemia, kidney stones and schizophrenia.

Despite of its wide applications, it has significant side effects to human health that cannot be ignored. Accidental consumption of MB can cause stomach upset, nausea, vomiting, diarrhoea and bladder irritation. This medication may lead to the urine or stool to turn green-blue. Moreover, MB induces serious side effects include fainting, dizziness, high fever, pale or blue skin color, irregular heartbeat and unusual tiredness, as well as itching or swelling of the face, tongue or throat and trouble breathing (Shodhganga, 2008).

2.2 Carbon Nanotubes

CNTs that were discovered by Sumio Iijima in 1991 had opened up a new area in the nanotechnology field. They are made up of multiple sheets of single-layer carbon atoms (graphene) that rolled up to form a cylindrical structure. Generally, CNTs were categorised into two types, which are SWCNT that having diameter below 1 nm and MWCNT with diameters equal or more than 100 nm.

The sp^2 bonds formed between the CNTs allows them to achieve molecular interaction that is as strong as their building block graphene. These sp^2 bonds and natural inclination of carbon nanotubes will join through Van der Waals forces, thereby producing materials with low weight and ultra-high strength. Moreover, these materials are having excellent thermal and electrical conductivity, which result in their application in various fields (Nanowerk, 2019). Figure 2.2 illustrated the schematic model of SWCNT and MWCNT

conceptually obtained from single graphene sheets, while the differences between SWCNT and MWCNT were stated in Table 2.2.
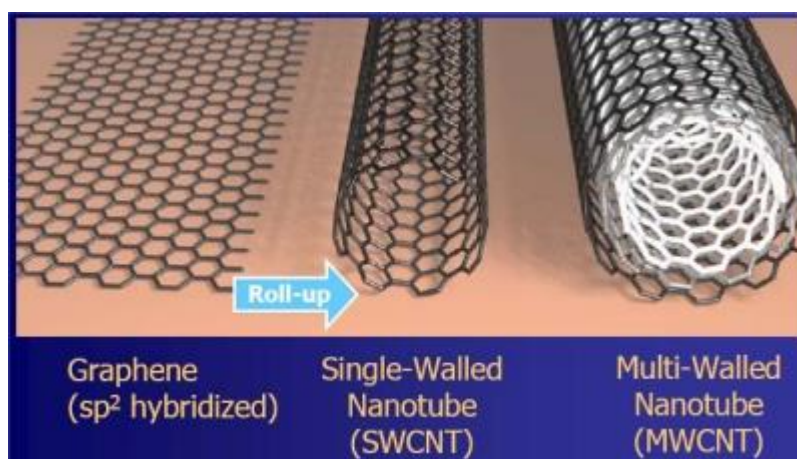
Figure 2.2: Schematic Model of SWCNT and MWCNT (Carrara, 2010).

Table 2.2: Comparison between SWCNT and MWCNT (Techinstro, 2018).

Properties	SWCNT	MWCNT
Layers	Single layer of graphene which forms a cylindrical shape	Multiple layers of graphene which formed in a concentric pattern around the smallest nanotube
Allotropic	Six-atom carbon rings in a hexagonal shape (identical to graphite)	Several tubes set in concentric layers in a cylindrical shape
Strength	Lower strength	Higher strength
Efficiency	Lower efficiency	Higher efficiency

MWCNTs were chosen in this study instead of SWCNTs due to their excellent properties, such as highly conductive, high aspect ratio with lengths typically more than hundred times the diameter, high tensile strength, as well as good thermal and chemical stability. Owing to their high conductivity, MWCNTs were widely employed in electrically conductive polymers and battery cathodes. Besides, high tensile strength of MWCNTs also played their

roles in structural laminates, aerospace applications and golf club shafts to improve the structural composites. Last but not least, the high aspect ratio, large specific surface area and high mechanical strength of MWCNTs had enabled them to be used in water filtration membranes as efficient filtration media (AzoNano, 2013).

2.3 Fe_3O_4 Nanoparticles

Iron oxides are common natural compounds, such as oxides, hydroxides and oxide-hydroxides. These minerals were synthesized by aqueous reactions under various redox and pH conditions. The basic compositions of iron oxides include Fe, O and/or OH. Though, different iron oxides have their particular valency of iron and overall crystal structure. Some of the well-known iron oxides are akageneite. magnetite (Fe_3O_4 nanoparticles), hematite, goethite and lepidocrocite (Bu, n.d.).

Recently, Fe_3O_4 nanoparticles have attracted much attention from many researchers due to their unique properties, such as large surface area, high surface energy, low toxicity, superparamagnetism, high absorption and easy separation methodology. It can be applied in the biomedical field for protein immobilization, for instance diagnostic magnetic resonance imaging (MRI), drug delivery and thermal therapy (Ali, et al., 2016). Besides, it can also be applied in water treatment, such as oily water treatment, heavy metal ions removal, absorption of toxic water soluble molecules, as well as residue pesticide determination and removal (Li, et al., 2011).

2.4 Magnetic MWCNTs

In recent years, researchers have paid much attention in the nanocomposites of MWCNT and Fe_3O_4 nanoparticles owing to their exclusive properties, particularly in nanoscale. Rahmawati, et al. (2017) stated that MWCNTs have enormous potential in many applications as it has high electric conductivity, large surface area, as well as mechanically and thermally stable. Simultaneously, Fe_3O_4 nanoparticles also owns unique magnetic properties, which known as superparamagnetic behaviours in nanoscale. Additionally, Fe_3O_4 nanoparticles has become an attractive material as it is flexible to be positioned according to

its size and structures. Figure 2.3 illustrated the MWCNTs-Fe$_3$O$_4$ nanocomposites.
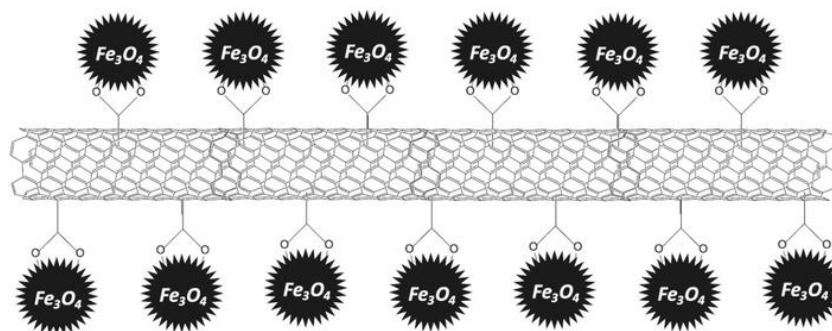
Figure 2.3: Illustration of MWCNTs-Fe$_3$O$_4$ Nanocomposites (Sadegh, Shahryari-ghoshekandi and Kazemi, 2014).

MWCNTs-Fe$_3$O$_4$ nanocomposites had been employed in many fields such as adsorbents, for removal trace arsenic and chromium, for immune sensor, for immunoscreening, for drug delivery, etc. Several methods can be used in the preparation of MWCNTs-Fe$_3$O$_4$ nanocomposites, for instance hydrothermal method, in situ chemical precipitation method and direct doping method.

It was important to remove the impurities of MWCNTs before the preparation of MWCNTs-Fe$_3$O$_4$ nanocomposites. Hence, the pristine MWCNTs were first suspended in concentrated nitric acid and reflux at 120 °C for 24 h. Then, the blank solution was filtered after cooling down to ambient temperature. The MWCNTs that obtained were rinsed with distilled water for multiple times until they reached a neutral pH value. After that, the moisture on the MWCNTs was removed in vacuum at 60 °C for future use (Zhong, et al., 2012; Huang, Yu and Jiang, 2014).

2.4.1 Hydrothermal Method

Zhong, et al. (2012) reported that the MWCNTs-Fe$_3$O$_4$ nanocomposites were synthesized by hydrothermal method. Firstly, a mixture of 200 mg of MWCNTs treated with HNO$_3$ and 15 mL of deionized water was sonicated for 15 min. Next, 4.5 mmol FeSO$_4 \cdot$7H$_2$O was then mixed with the solution with the addition of 5 ml polyethylene glycol solution. The solution was obtained under vigorous stirring at 30 °C by adding diluted ammonia with a volume of 15 mL. The

reaction was carried out at a pH value of 10. Upon adding 0.135 mL 30 % H_2O_2 into the solution slowly, a homogenous mixture was obtained by stirring the mixture for around 10 min. The slurry that formed previously was then transferred into a Teflon-lined autoclave of 50 mL in volume. A furnace was used to heat the slurry at a temperature of 160 °C for 5 h. MWCNTs-Fe_3O_4 nanocomposites were recovered from the reaction mixture by using 6000 G permanent magnet after it was cooled to ambient temperature. Lastly, the MWCNTs-Fe_3O_4 nanocomposites were rinsed with ethanol and water for three time, and dried under vacuum condition for 12 h at temperature of 80 °C. Figure 2.4 depicted the schematic illustration of the decoration of MWCNTs with Fe_3O_4 nanoparticles in the hydrothermal system.
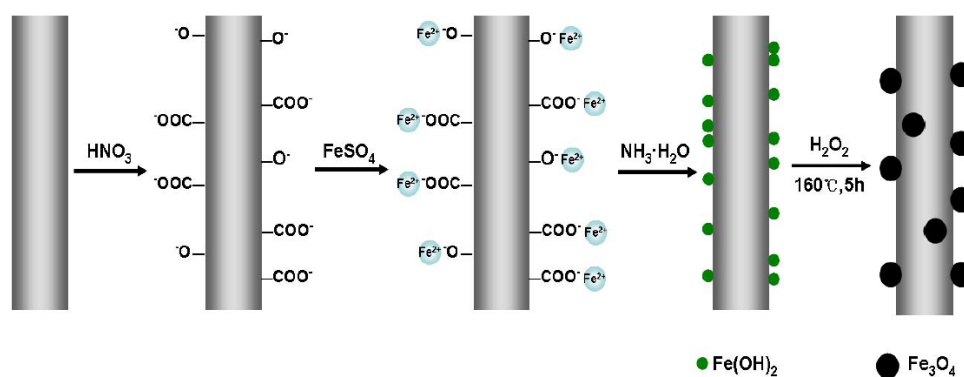
Figure 2.4: Schematic Illustration of the Decoration of MWCNTs with Fe_3O_4 Nanoparticles in the Hydrothermal System (Zhong, et al., 2012).

2.4.2   In Situ Chemical Precipitation Method

According to Song, et al. (2011), SDS adsorbed MWCNTs were obtained by dispersing MWCNTs in SDS aqueous solution (1 wt.%) where ultrasonication was ran for 2 h to modified the surface of MWCNTs, followed by further washing with deionized water and drying. After dissolving 0.47 g of $FeCl_3.6H_2O$ and 0.11 g of $FeCl_2$ in a flask containing 20 mL deionized water, 0.15 g of SDS adsorbed MWCNTS were transferred into the flask. The mixture was stirred vigorously under argon atmosphere. Under vigorous stirring, ammonia solution with concentration 1.5 M was added dropwise into the mixture after 5 min till it reached pH 8. Without stirring, the mixture was reacted at 60 °C for 2 h. Lastly, MWCNTs-Fe_3O_4 nanocomposites were obtained as final

products and were washed with deionised water repetitively. The products will be dried at 80 °C for 12 h.

2.4.3 Direct Doping Method

According to Stoffelbach, et al. (2005) and Cheng, et al., 2008, MWCNTs-Fe_3O_4 nanocomposites can be prepared by simply adding both oppositely charged Fe_3O_4 nanoparticles (positive) and MWCNTs (negative) together. The first step of this method includes the generation of carboxylic acid, -COOH at the surface of MWCNTs. Then, the positively charged Fe_3O_4 nanoparticles were therefore anchored to MWCNTs-COOH by using the concept of opposite electrostatic attraction. Figure 2.5 showed the interaction between Fe_3O_4 and -COOH on the surface of MWCNTs.
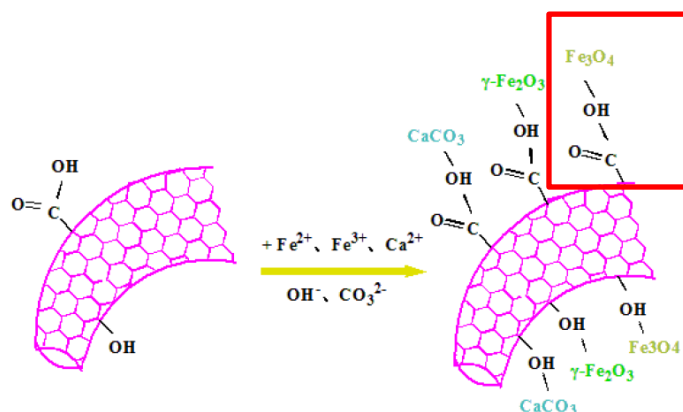
Figure 2.5: Interaction between Fe_3O_4 Nanoparticles with -COOH on the Surface of MWCNTs (Li, et al., 2017).

2.5 Characterisation of MWCNTs-Fe_3O_4 Nanocomposites

2.5.1 Fourier Transform Infrared

FTIR spectroscopy was utilized to identify the species that absorbed on the catalyst surface so as to study the way of chemisorption of these species. Selen, et al. (2015) had identified the functional groups on the MWCNTs surface by using a FTIR spectroscopy in a range of 400 and 4000 cm^{-1} by avenging 16 scans. It was reported that the adsorption of MB on MWCNTs was significantly affected by the functional groups of MWCNTs, which included C=O stretching (carboxyl groups), bonded -OH groups (phenols and alcohols), C-H stretching (non-ionic carboxyl groups), C-H bending (methyl and phenyl alcohols), C=C

stretching (aromatic ring), C-O stretching (ether groups), and -C-C- group. Huang, Yu and Jiang (2014) futher reported that an intense band around 577 cm^{-1} was shown in the spectra of MWCNTs-Fe$_3$O$_4$ nanocomposites arises from the stretching vibration of Fe-O-Fe, which proved that the Fe$_3$O$_4$ nanoparticles were decorated onto the MWCNTs. The absorption peaks of the MWCNTs-Fe$_3$O$_4$ nanocomposites were summarised in the table below.

Table 2.3: FTIR Spectra Characteristics of MWCNTs-Fe$_3$O$_4$ Nanocomposites (Huang, Yu and Jiang, 2014; Selen, et al., 2015).

IR peak	Frequency (cm^{-1})	Assignment
1	3409	Bonded -OH group
2	2927	C-H stretching
3	1719	C=O stretching
4	1624	C=C stretching
5	1385	C-H bending
6	1186	C-O stretching
7	1112	C-O stretching
8	1044	-C-C- group
9	783.1	-C-C- group
10	577	Fe-O-Fe stretching

2.5.2 X-ray Powder Diffraction

XRD was commonly applied to determine the crystallite size and structure of crystalline phase. On the other hand, the crystallite size of the sample can be measured through Scherrer's Formula by utilizing the width of the peak.

$$< L >= \frac{K\lambda}{\beta \cos\theta} \tag{2.1}$$

where

L = a measure of the dimension of the particle in the direction perpendicular to the reflecting plane

λ = the X-ray wavelength

K = a constant (often take as 1)

β = the peak width

θ = the angle between the beam and the normal to the reflecting plane

X-ray diffractometer was used to determine the phase structure of the nanocomposites with Cu Kα radiation with a wavelength of 0.15406 nm. The incident radiation was scanned at a rate of $0.02°$ s^{-1} while the diffractogram was measured in the angle of 2θ between 10° and 80° (Song, et al., 2011) and from 20° to 90° (Hernandez, et al., 2015). Song, et al. (2011) reported that the characteristic peak that appeared at 2θ angle of 26.05° was ascribed to MWCNTs, while the peaks at 2θ angle of 32.0°, 35.5°, 43.2°, 53.8° and 62.9° were correlated to the crystal planes (220), (311), (400), (422) and (440) of face-centred cubic (FCC) Fe_3O_4 nanoparticles. From the Scherrer's Formula, the mean particle size for Fe_3O_4 nanoparticles was calculated as 14 nm.

2.5.3   Scanning Electron Microscope with Energy Dispersive X-Ray

The surface morphology of the nanocomposites was observed by SEM-EDX. Madrakian, et al. (2011) realved that the diameter of MWCNTs-Fe_3O_4 nanocomposites was around 58 nm by using a SEM at voltage of 15 kV. Other researchers claimed that the diameter of the MWCNTs decorated with Fe_3O_4 nanoparticles was about 50 to 80 nm. The SEM images in Figure 2.6 showed that the tubular structure of the MWCNTs was not destructed by the decoration process (Huang, Yu and Jiang, 2014).
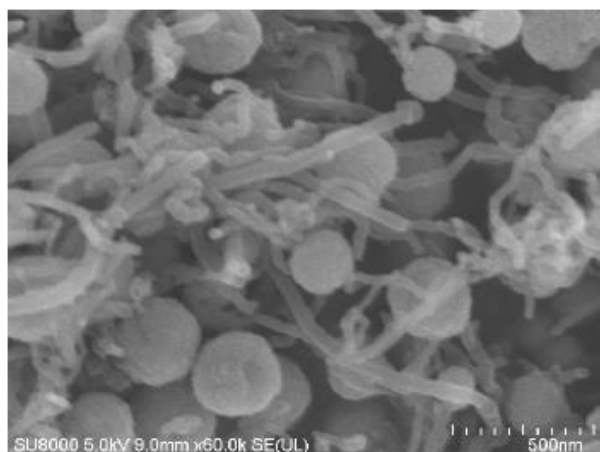
Figure 2.6: SEM Image of MWCNTs-Fe_3O_4 Nanocomposites (Huang, Yu and Jiang, 2014).

2.5.4 Brunauer-Emmett-Teller

Madrakian, et al. (2011) reported that the specific surface areas, which also known as BET surface areas of the magnetic MWCNTs were studied by applying the concept of Brunauer, Emmett and Teller (BET). The BET technique determines the surface area of the magnetic MWCNTs by adsorbing the nitrogen moelcules on the surface at the temperature of -196 °C. The subsequent desorption of the nitrogen molecules will be measured and the surface area can be calculated by multiplying the number of nitrogen molecules desorbed with the surface area of one nitrogen molecule (0.162 nm^2). On top of that, the pore volume and pore diameter distribution of the magnetic MWCNTs were derived from Barrett-Joyner-Halenda (BJH) model. The results showed that the magnetic MWCNTs had an average specific surface area of 144.68 m^2/g, which was larger than that of MWCNTs (44.29 m^2/g). This was mainly due to addition of Fe_3O_4 nanoparticles onto the surface of the MWCNTs. Other than that, the results from Hu, et al. (2011) stated that the specific surface area of magnetic MWCNTs and Fe_3O_4 nanoparticles was found to be 20.58 m^2/g and 10.85 m^2/g respectively.

2.5.5 Thermogravimetric Analysis

In this study, TGA analysis was used to characterise the thermal stability of the magnetic MWCNTs by monitoring the mass of the sample against temperature. The research carried out by Yu, et al. (2012) reported that the TGA curves were obtained at the temperature range between 40 °C and 900 °C under the heating rate of 10 °C/min in air. The ramp rate of the temperature is usually range from 1 to 20 °C/min. However, intermediate ramp rate was preferable because at high ramp rate, the moisture inside the catalyst will expand very fast and this might pressurise and break the wall of the catalyst pores. In result, the catalyst will be destroyed and lead to an inaccurate result. According to Sadegh, Shahryari-ghoshekandi and Kazemi (2014), magnetic MWCNTs experienced a weight loss at a lower temperature range from 490 °C to 635°C as compared to the pristine MWCNTs, leaving the residue weight of Fe_3O_4 nanoparticles at around 26.65 % as shown in Figure 2.7. This was because the catalytic role of Fe_3O_4 nanoparticles reduced the weight loss of magnetic MWCNTs during the oxidation process.
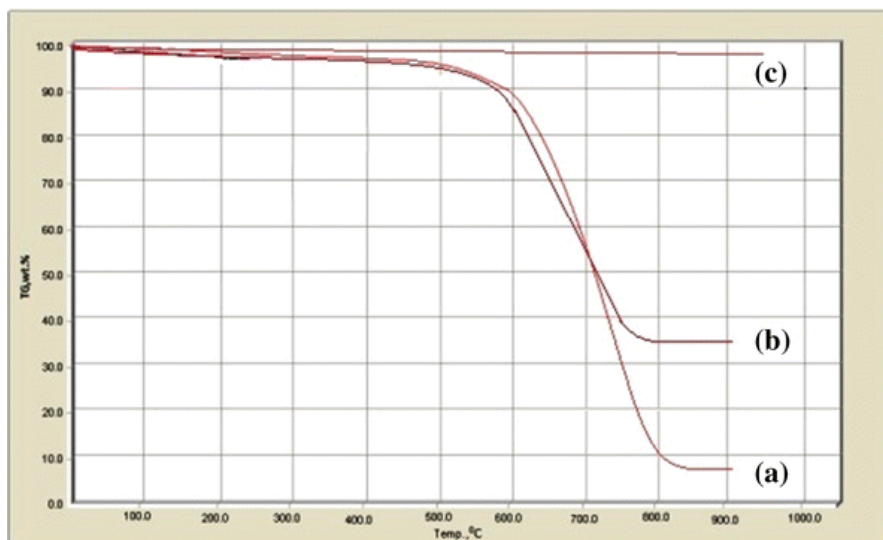
Figure 2.7: TGA Curves of (a) MWCNTS, (b) Magnetic MWCNTS, and (c) Fe₃O₄ Nanoparticles (Sadegh, Shahryari-ghoshekandi and Kazemi, 2014).

2.6 Adsorption

Adsorption was known as the deposition of molecular species onto the surface, and therefore it is a surface phenomenon. It happened when the adsorptive gets attached onto the surface of the adsorbents by physical forces or chemical bonds and forms the adsorbate. Desorption is the converse of adsorption in which the adsorbate was removed from the surface of adsorbent. Figure 2.8 showed the adsorption and desorption process.
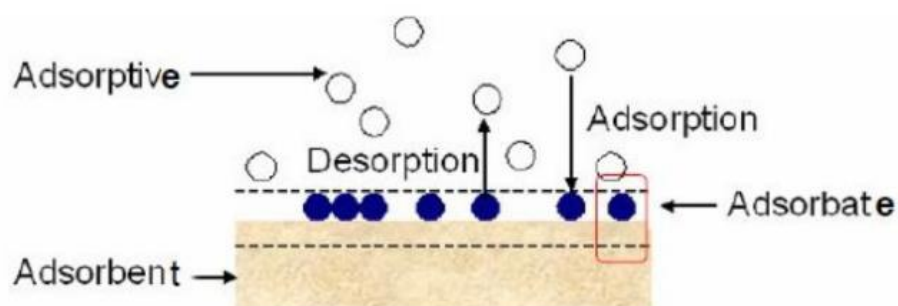
Figure 2.8: Illustration of Adsorption and Desorption Process (Dwivedi, 2016).

2.6.1 Mechanism of Adsorption

Adsorption is an exothermic process which means that the enthalpy change is always negative. Enthalpy of adsorption is defined as the amount of heat changed when one more of the adsorbate is adsorbed on the adsorbent. The

entropy is decreased when the molecules of adsorbate are decorated on the surface of the adsorbent, restricting the free movement of the molecules. Adsorption occurs spontaneously at constant temperature and pressure, and thus Gibb's free energy is also decreased (eMedicalPrep, 2019).

Adsorption is dependent on various parameters, such as temperature, pH, size, sorbent dose and surface morphology. It also depends on sorbate structure and concentration. Figure 2.9 showed the mechanism of adsorption.
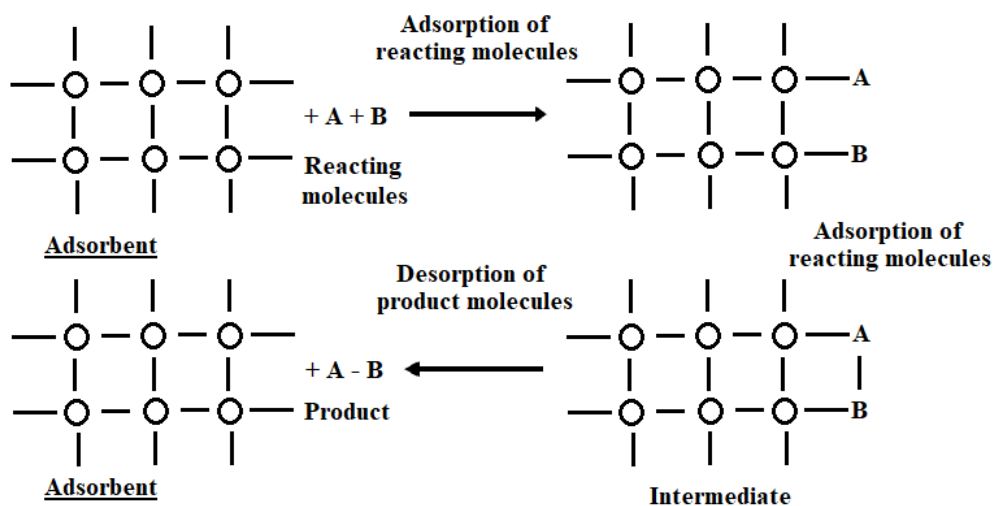
Figure 2.9: Mechanism of Adsorption (Anusha, 2013).

2.6.2   Adsorption of MB by MWCNTs-Fe₃O₄ Nanocomposites

According to Ghaffar and Younis (2015), the positive charge of MB in aqueous solution is attributed to the C-C double bonds as well as the π-electrons. The π-electrons on MB can form hydrophobic interactions through the π- π electron coupling with the electrons originate from benzene rings on surface of MWCNTs. Therefore, MB may interact with the side wall, such as on the axis direction of the MWCNTs. The electrostatic attraction also assists in MB adsorption using MWCNTs. The negative charges of the carboxyl group on the surface of MWCNTs will attract the positively charge MB in the solution, resulting in the adsorption of MB by MWCNTs. Figure 2.10 illustrated the general adsorption sites and the types of interaction between MWCNTs and MB dyes.
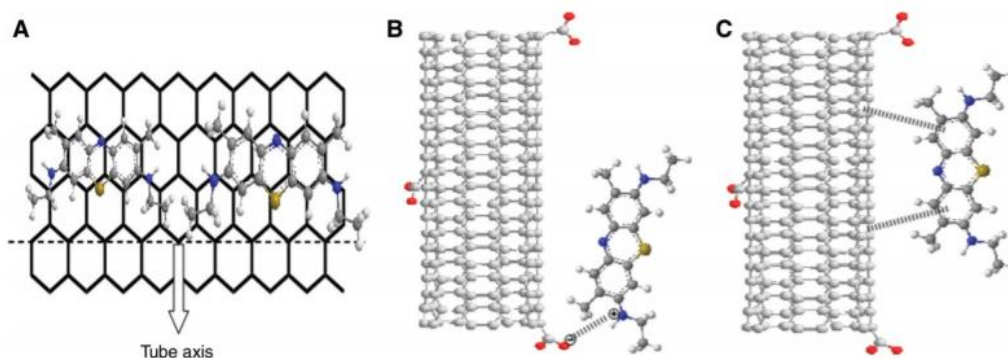
Figure 2.10: Schematic Illustration of Typical Adsorption Sites and the Possible Interaction between MWCNTs and MB Dyes: (A) axis direction; (B) electrostatic attraction and (C) π- π stacking (Ghaffar and Younis, 2015).

2.7   Parameters for Adsorption of MB

2.7.1   pH

The pH value of the solution shows significant impact on the adsorption of MB using MWCNTs-Fe$_3$O$_4$ nanocomposites. It would affect both surface binding-sites and aqueous chemistry of the adsorbent. Rajabi, Mahanpoor and Moradi (2017) expressed that a cationic dye prefers high pH value whereas an anionic dye favours a low pH value. According to Madrakian, et al. (2011), the impact of pH on the removal of MB was examined between 4 and 12. The initial dye concentration was fixed at 20 mg L^{-1}. The effect of pH was also studied by Huang, Yu and Jiang (2014) over a range of 4 to 10. The surface of MWCNTs-Fe$_3$O$_4$ nanocomposites was negatively charged as pH increased above 2 and thus the nanocomposites can capture positively charged MB by electrostatic attraction. Theoretically, higher pH will result in larger negative charge on MWCNTs-Fe$_3$O$_4$ nanocomposites, and therefore higher removal efficiency of MB. However, the results carried out by Huang, Yu and Jiang (2014) and Madrakian, et al. (2011) showed that the pH values of 6 to 7 were best for the removal of MB. This can be probably due to the increase in competition between OH$^-$ and the limited adsorption sites on MWCNTs-Fe$_3$O$_4$ nanocomposites surface for the adsorption of MB under alkaline condition.

2.7.2   Initial MB concentration

The initial MB concentration has huge influence on the removal of MB. Selen, et al. (2015) investigated the initial MB concentration in a range of 20 to 60

mg/L, with the value of other parameters were kept constant. It showed that higher removal percentage of MB can be achieved when the initial MB concentration is high, which can be accredited to the present of higher number of MB dye molecules. The MB concentration is vital to produce the driving force for the dyes to conquer the mass transfer resistance that presence between the aqueous and solid phases. Nevertheless, an increase in initial MB concentration will reduce the efficiency of MB removal as the available adsorption sites on the MWCNTs-Fe_3O_4 nanocomposites are saturated with dyes. Hence, there will be insufficient sites for the MB molecules to adsorb.

2.7.3   MWCNTs-Fe_3O_4 Nanocomposites Dosage

The dosage of adsorbent is another significant parameter in determining the removal percentage of MB. Malayeri, Sohrabi and Ghourchian (2012) had conducted an experiment by using 1 mg/L of dye exposed to 1 to 3 mg of MWCNTs-Fe_3O_4 nanocomposites and the results revealed that the adsorption capacity was the highest in 1 mg of nanocomposites. Besides that, adsorbent quantity of 2.5 to 22.5 mg was also tested by Huang, Yu and Jiang (2014) by keeping the other parameters constant. The results showed that higher adsorbent dosage will contribute to higher removal rate of dye. This is probably due to the increase in adsoption sites as the surface area of the adsorbent is increased. Meanwhile, the adsorption capacity is decreasing with increasing adsorbent doasge owing to the reduction of the unit adsorption.

2.8   Heterogeneous Fenton-like Degradation

Classic Fenton that consists of a ferrous salt, so called Fenton reagent (Fe^{2+}) and H_2O_2, was an effective oxidant for a variety of organic compound as Fe^{2+} and H_2O_2 are environmentally friendly. H_2O_2 activation can simply occur at room temperature under atmospheric pressure in a short reaction time. However, this reaction is strongly dependent on the pH. Hence, it needs large amount of acid to maintain the pH to the optimum of 3, and the successive neutralization will lead to sludge formation. Additionally, it also requires large amount of Fe^{2+} and H_2O_2 to keep the system active. In this case, studies based on new methods such as Fenton-like degradation that replaced Fe^{2+} ions with Fe^{3+} ions to generate

reactive $\cdot$OH radicals, have therefore received much attention among the researchers recently.

The mechanisms of heterogeneous Fenton-like degradation were shown below by reacting Fe^{3+} ions with H_2O_2 (Pereira, Oliveira and Murad, 2012).

$$Fe^{3+} + H_2O_2 \rightarrow FeOOH^{2+} + H^+ \tag{2.2}$$

$$FeOOH^{2+} \rightarrow Fe^{2+} + \cdot OH \tag{2.3}$$

$$Fe^{3+} + \cdot OOH \rightarrow Fe^{2+} + O^2 + H^+ \tag{2.4}$$
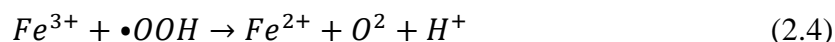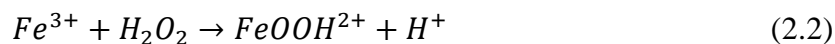
2.8.1 Heterogeneous Fenton-like Degradation of MB

Mechanisms of heterogeneous Fenton-like degradation of MB are listed in Equation (2.5) to (2.8). First, the $\equiv Fe^{III}\cdots H_2O_2$ and $\equiv Fe^{II}\cdots H_2O_2$ precursor surface complexes are formed by absorbing the H_2O_2 on the Fe_3O_4 nanoparticles surface. The absorption of H_2O_2 on the Fe_3O_4 surface may form two surface coordinates that are an inner- or an outer-sphere as shown in Equation (2.5) and (2.6) respectively. The electron transfer within $\equiv Fe^{III}\cdots H_2O_2$ could produce $\equiv Fe^{II}$ species and $\cdot O_2H$ radicals as indicated in Equation (2.5), while the electron transfer within $\equiv Fe^{II}\cdots H_2O_2$ species will yield $\equiv Fe^{III}$ and $\cdot OH$ radicals as presented in Equation (2.6). The high oxidizing ability of the formed $\cdot O_2H$ radicals and $\cdot OH$ radicals will immediately bind to MB, resulting in the degradation and mineralization of MB as shown in Equation (2.7) and (2.8) (Jiang, et al., 2011).

$$\equiv Fe^{III} + H_2O_2 \leftrightarrow Fe^{III\cdots}H_2O_2 \rightarrow H^+ + \equiv Fe^{II} + \cdot O_2H \tag{2.5}$$

$$\equiv Fe^{II} + H_2O_2 \leftrightarrow Fe^{II\cdots}H_2O_2 \rightarrow OH^- + \equiv Fe^{III} + \cdot OH \tag{2.6}$$

$$MB + \cdot OH \rightarrow\rightarrow CO_2 + H_2O \tag{2.7}$$

$$MB + \cdot O_2H \rightarrow\rightarrow CO_2 + H_2O \tag{2.8}$$
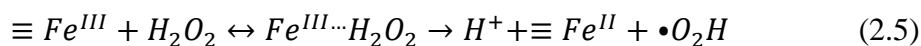
2.9 Parameters for Heterogeneous Fenton-like Degradation of MB

2.9.1 pH

The solution pH plays a vital role in the degradation of MB by MWCNTs-Fe_3O_4 nanocomposites. The experiments conducted by Jiang, et al. (2011) and Fayazi, et al. (2016), which involved the degradation of MB at the pH range of 2 to 10.5

and 3 to 9, revealed that the optimum degradation efficiency was found at the pH range of 3 to 5. This is caused by the rapid dissolved of Fe_3O_4 nanoparticles at the pH below 3. Moreover, the oxidation potential of •OH is lower in weak acidic or alkaline aqueous solution.

2.9.2 Initial Concentration of MB

The effect of various initial MB concentration was investigated by Ahmed, et al. (2015) and Singh, et al. (2018) in a range of 5 to 40 mg/L. The results indicated that the degradation efficiency was decreased with increasing initial MB concentration. This is mostly caused by the reduction of active sites on the catalyst surface as they are being occupied by the MB molecules. Therefore, it resulted in lesser •OH radicals on the surface of catalyst, causing the rate of MB degradation to decrease.

2.9.3 MWCNTs-Fe₃O₄ Nanocomposites Dosage

The influence of adsorbent dosage on the Fenton reaction of MB was studied by the researchers in a range of 0 to 3 g/L under the conditions where other parameters were remained constant (Hu, et al., 2011; Fayazi, et al., 2016; Jiang, et al., 2011). The results illustrated that the greater the adsorbent dosage, the higher the number of active sites available for the formation of •OH radicals, thereby enhancing the degradation efficiency of MB.

2.9.4 H₂O₂ Concentration

The concentration of H_2O_2 oxidant is a significant aspect in Fenton-like degradation as it is directly correlated to the number of •OH radicals generated in Fenton reaction. Based on Fayazi, et al. (2016), the influence of concentration of H_2O_2 on the degradation of MB was studied in the range of 4 to 16 mmol/L. According to the result, the degradation efficiency improved as the H_2O_2 concentration raised from 4 to 12 mmol/L, but remain almost constant from 12 to 16 mmol/L. Ahmed, et al. (2015) also performed the degradation of MB by varying the quantity of H_2O_2 concentration from 0.5 mmol/L to 10.0 mmol/L and the results stated that the optimum degradation efficiency happened at 3 mmol/L of H_2O_2 concentration. The increased in the degradation efficiency is mainly credited to the increased in the amount of radicals formed, whereas there

is no significant increased of degradation efficiency in higher concentration of H_2O_2 due to the scavenging effects of H_2O_2 as shown in Equation (2.9) and (2.10). From the equations, it can be seen that the excess H_2O_2 will compete with MB to react with the •OH radicals, lessening the reactive radicals available for the degradation of MB. The reaction between the excess H_2O_2 and the •OH radicals will form water and hydroperoxyl radicals (•OOH), which has a lower oxidation potential as compared to the •OH radicals and thus do much less contribution to the degradation of MB.

$$H_2O_2 + •OH \rightarrow H_2O + •OOH \qquad (2.9)$$

$$•OOH + •OH \rightarrow H_2O + O_2 \qquad (2.10)$$

2.10   Design Expert Simulation

Design Expert is widely employed to design and interpret multi-factor experiments. It covers a wide range of designs, for instance composite designs, factorials and fractional factorials. It can be used to optimize the problem with both process variables and mixture variables. The software is also capable of detecting cases where standard designs are not relevant by generating D-optimal designs, or where users wish to improve an existing design (Buxton, 2007).

Design Expert is specifically devoted to perform design of experiments (DOE). DOE allows users to change the input factors of the process with the intention of observing the consequences on the output. DOE has been practised in every industry, including hard goods manufacturing, agricultural, pharmaceutical, automotive, chemical, etc. Service industries have also gained benefits by obtaining data from their process and analysing it appropriately (Stat-Ease, 2017).

Design Expert is also equipped with tools to outline an ideal experiment on the mixture, process or combination of components and factors. Besides, it makes thing to be seen easily if anything appears as statistically significant and provides a direction on how to achieve the most precise results. It offers the confidence that users need to present or publish their findings. Lastly, Design Expert also gives a vast choice of graphs that assist users to identify standout effects and visualize their results. Its outputs develop a strong impression when users communicate their findings to supervisors and peers (Stat-Ease, 2017).

CHAPTER 3

METHODOLOGY AND WORK PLAN

3.1   Flowchart

Synthesis of MWCNTs-Fe_3O_4 nanocomposites

- Purify with HNO_3
- Prepare the nanocomposites via direct doping

Characterizations of MWCNTs-Fe_3O_4 nanocomposites

- FTIR
- XRD
- SEM-EDX
- BET
- TGA

Adsorption of MB

- Effect of pH
- Effect of initial MB concentration
- Effect of MWCNTs-Fe_3O_4 nanocomposites dosage

Heterogeneous Fenton-like Degradation of MB

- Effect of pH
- Effect of initial MB concentration
- Effect of MWCNTs-Fe_3O_4 nanocomposites dosage
- Effect of H_2O_2 concentration

3.2   Materials and Apparatus

The instruments that were used in this study include XRD, FTIR, FESEM-EDX, BET and TGA to characterised the magnetic MWCNTs, as well as UV-Vis to identify the concentration of MB. The list of apparatus and materials that were used in this study were listed in the tables below.

Table 3.1: List of Apparatus.

Apparatus	Purpose of use
Magnet hot plate	To heat up the mixture of pristine MWCNTs and nitric acid
Oven	To dry magnetic MWCNTs after rinsed with distilled water
pH meter	To measure the pH of the solution
Mini-rotator	To achieve uniform mixing of MWCNTs with Fe_3O_4 nanoparticles
Microbalance	To measure the weight of MWCNTs in mg
Sonicator	To use for the dispersion of MWCNTs in solution with Fe_3O_4 nanoparticles
Orbital shaker	To achieve uniform mixing of magnetic MWCNTs with MB

Table 3.2: List of Materials.

Chemicals	Purity (%)	Supplier	Purpose of use
MWCNTs	> 95	Fisher Scientist Malaysia	To synthesis magnetic MWCNTs
Nitric Acid	65	Merck, Malaysia	To act as oxidising agent and remove impurities of MWCNTs

Table 3.2 (Continued)

Fe₃O₄	100	Merck, Malaysia	To synthesis magnetic MWCNTs
MB	-	Merck, Malaysia	To act as adsorbate
Ethanol	> 99.5	Sigma-Aldrich	To desorb MB from magnetic MWCNTs
Potassium bromide	> 99	Sigma-Aldrich	To mix with sample in FTIR analysis
Dilute HCl	37	Sigma-Aldrich	To adjust the pH
Dilute NaOH	20	Sigma-Aldrich	To adjust the pH

3.3 Preparation of Magnetic MWCNTs

3.3.1 Purification of MWCNTs

Purification of MWCNTs is crucial in the preparation of MWCNTs in order to remove the impurities of the pristine MWCNTs. Typically, 1 g of untreated MWCNTs were dispersed in 100 mL of concentrated nitric acid (HNO_3) with the aid of ultrasonication treatment for 1 h. Then, the mixture was heated up to 80 °C for 6 h. After being filtered and cleaned with distilled water to neutralize the MWCNTs, the purified MWCNTs were dried at 80 °C overnight to obtained the acid purified MWCNTs (MWCNTs-COOH).

3.3.2 Synthesis of MWCNTs-Fe₃O₄ Nanocomposites

The MWCNTs-Fe₃O₄ nanocomposites were prepared by direct doping method. Firstly, MWCNTs-COOH and Fe₃O₄ nanoparticles with a ratio of 1.5:1 was dispersed in 15 mL of deionize water respectively with the aid of ultrasonication for 30 min. Before adding the Fe₃O₄ nanoparticles to MWCNTs-COOH, the pH of both dispersions was adjusted to 4.5 - 4.6. After that, the mixture was homogeneously dispersed 5 min under ultrasonication. The mixture was then rotated overnight in a mini-rotator to achieve uniform mixing. Upon completion

of mixing, the products were magnetically collected via a magnet for 30 min, and rinsed with distilled water thoroughly. Finally, the collected MWCNTs-Fe_3O_4 nanocomposites were dried at 80 °C overnight in an oven.

3.4 Characterisation of MWCNTs-Fe_3O_4 Nanocomposites

3.4.1 FTIR Analysis

FTIR spectra were obtained using a PerkinElmer Infrared Spectrometer to identify the functional group of the pristine MWCNTs, MWCNTs-COOH and MWCNTs-Fe_3O_4 nanocomposites. The analysis was usually attempted with the mixture of samples and potassium bromide (KBr). After drying the samples and KBr in an oven overnight, 1 g of KBr was added to 3 mg of samples. The mixture was then grinded by a motar to finely grounded particles to minimize the scattering losses and distortion of adsorption band. Next, the mixture was shaped into transparent disk before placing it in the sample holder. Lastly, FTIR analysis was carried out over 32 cumulative scans within the wavenumber of 4 000 to 400 cm^{-1}.

3.4.2 XRD Analysis

The phase structures of the pristine MWCNTs, MWCNTs-COOH, Fe_3O_4 nanoparticles, MWCNTs-Fe_3O_4 nanocomposites and spent MWCNTs-Fe_3O_4 nanocomposites were determined by XRD-6000 X-ray diffractometer (Shimadzu, Japan) with Cu Kα radiation (λ = 0.15406 nm). The XRD peaks were collected in a 2θ range from 10° to 80° with a scanning rate of 0.02 s^{-1}. Before locating the sample into a sample holder, it was grounded. The changes in the intensities of X-rays that caused by the diffraction of the X-rays were recorded continuously by focusing the X-rays on the sample. By assuming the samples were spherical, the crystallite size was estimated by Scherrer formula.

3.4.3 SEM-EDX Analysis

The surface morphology and aligned feature of the pristine MWCNTs, MWCNTs-COOH and MWCNTs-Fe_3O_4 nanocomposites were characterized using FESEM-EDX at 15 kV. The samples were first dispersed in ethanol and ultrasonicated for 5 min. After dropping the sample solution on the silicon slide with a glass dropper, it was then dried at 40 °C prior to SEM-EDX analysis.

3.4.4 BET Analysis

The specific surface area of the pristine MWCNTs, MWCNTs-COOH and MWCNTs-Fe$_3$O$_4$ nanocomposites were characterized using an 3Flex Physisorption. At first, 0.1 g of sample was placed inside the tube for degassing process at 250 °C. After that, the samples were immersed into the liquid N$_2$ at -196 °C for the adsorption and desorption process.

3.4.5 TGA Analysis

The thermal stability of the MWCNTs-COOH and MWCNTs-Fe$_3$O$_4$ nanocomposites were studied by using a TA Instruments SDT Q600. Generally, the powder samples were placed inside the alumina crucibles during the analysis. By referring to the analysis condition carried out by Yu, et al. (2012) and Sadegh, Shahryari-ghoshekandi and Kazemi (2014), the nanocomposites were heated from room temperature to 1000 °C at a temperature ramp rate of 10 °C/min.

3.5 Design Expert Simulation

A response surface method coupled with CCD in Design Expert with 30 simulations test was simulated to determine the four process parameters that affect the percentage of adsorption and degradation of MB. The four process parameters included pH, initial MB concentration, MWCNTs-Fe$_3$O$_4$ nanocomposites dosage and H$_2$O$_2$ concentration. The four numeric factors and their respective coded and actual values were recorded in the Table 3.3.

Table 3.3: Coded and Actual Values of Process Parameters in CCD.

Factors	Code	Units	Level				
			$-\alpha$	-1	0	$+1$	$+\alpha$
pH	A	-	2	4	6	8	10
Initial MB concentration	B	mg/L	10	20	30	40	50
MWCNTs-Fe$_3$O$_4$ Nanocomposites Dosage	C	mg	10	15	20	25	30
H$_2$O$_2$ Concentration	D	mmol/L	5	8.75	12.5	16.25	20

After keyed in all the four parameters, 30 runs were generated randomly by the Design Expert as shown in Figure 3.4. With the simulated runs, laboratory experiments were carried out to obtain the percentage of adsorption and degradation for each set of runs.

Table 3.4: Experimental Matrix in Design Expert.

Run	A: pH	B: Initial MB Concentration (mg/L)	C: MWCNTs-Fe_3O_4 Nanocomposites Dosage (mg)	D: H_2O_2 Concentration (mmol/L)
1	6	50	20	12.5
2	6	30	20	12.5
3	4	20	15	8.75
4	4	20	25	8.75
5	4	40	25	16.25
6	6	30	20	5
7	4	40	15	8.75
8	8	20	15	8.75
9	6	30	10	12.5
10	6	30	20	12.5
11	8	40	15	16.25
12	8	40	15	8.75
13	6	30	20	12.5
14	8	20	25	8.75
15	6	30	20	12.5
16	4	40	15	16.25
17	6	10	20	12.5
18	2	30	20	12.5
19	8	40	25	16.25
20	8	20	25	16.25
21	6	30	20	12.5
22	4	40	25	8.75
23	6	30	20	20
24	6	30	30	12.5

Table 3.4 (Continued)

25	8	20	15	16.25
26	6	30	20	12.5
27	4	20	15	16.25
28	4	20	25	16.25
29	8	40	25	8.75
30	10	30	20	12.5

3.6 Simultaneous Adsorption and Degradation of MB

The simultaneous adsorption and degradation experiment were carried out at room temperature in a glass bottle containing 15 mL of MB exposed to 20 mg of MWCNTs-Fe_3O_4 nanocomposites as adsorbent (used Run 1 in Table 3.4 as an example). The pH was adjusted to 6 by HCl or NaOH solution. After shaking in the orbital shaker for 15 min for adsorption process to carry out, 12.5 mmol/L H_2O_2 was introduced into the reaction solution to initiate the degradation of MB. Then, the mixture was again shaken inside the orbital shaker for 5 h for the adsorption and degradation process to perform. After 5 h, MWCNTs-Fe_3O_4 nanocomposites were separated from MB solution using a permanent magnet for 30 min. At this stage, the equilibrium MB concentration will be determined by using UV-Vis spectrophotometer at 660 nm (λ_{max} of MB). The adsorption capacity at equilibrium (q_e) will be calculated using Equation (3.1) and the removal percentage of MB will be estimated using Equation (3.2). The concentration of MB at this point was estimated by Equation (3.3).

$$q_e = \frac{(C_o - C_e)V}{W} \qquad\qquad (3.1)$$

where

q_e = amount of MB adsorbed at equilibrium (mg/g)

C_o = initial concentration of MB (mg/L)

C_e = equilibrium concentration of MB (mg/L)

V = volume of MB solution (L)

W = weight of the adsorbent (g)

$$Removal\ \% = \frac{(C_o - C_e)}{C_o} \times 100 \tag{3.2}$$

$$C_T = C_o - C_{o,5h} \tag{3.3}$$

where

C_T = total concentration of MB being adsorbed and degraded (mg/L)

C_o = initial concentration of MB (mg/L)

$C_{o,5h}$ = concentration of MB after 5 h (mg/L)

To measure the amount of MB being degraded, the collected MWCNTs-Fe$_3$O$_4$ nanocomposites will be mixed with 20 mL ethanol solution and ultrasonicated for 30 min. Then, the MB concentration in the ethanol solution will be analysed by UV-Vis spectrophotometer at 660 nm using ethanol as blank solution. Equation (3.4) was used to calculate the concentration of MB that was degraded. The adsorption and degradation experiments were carried out for all the 30 runs as stated in Table 3.4.

$$C_{degraded} = C_T - C_{adsorbed} \tag{3.4}$$

where

$C_{adsorbed}$ = concentration of MB being adsorbed (mg/L)

$C_{degraded}$ = concentration of MB being degraded (mg/L)

CHAPTER 4

RESULTS AND DISCUSSION

4.1   Characterisation

Several techniques such as FTIR, XRD, SEM-EDX, BET and TGA were employed to characterize the functional group, phase structure, surface morphology, specific surface area, as well as the thermal stability of the pristine MWCNTs, MWCNTs-COOH and MWCNTs-Fe_3O_4 nanocomposites that synthesized by direct doping method.

4.1.1   FTIR Analysis

FTIR spectra of the pristine MWCNTs, MWCNTs-COOH and MWCNTs-Fe_3O_4 nanocomposites in Figure 4.1 were identified and the significant peaks were summarised in Table 4.1.
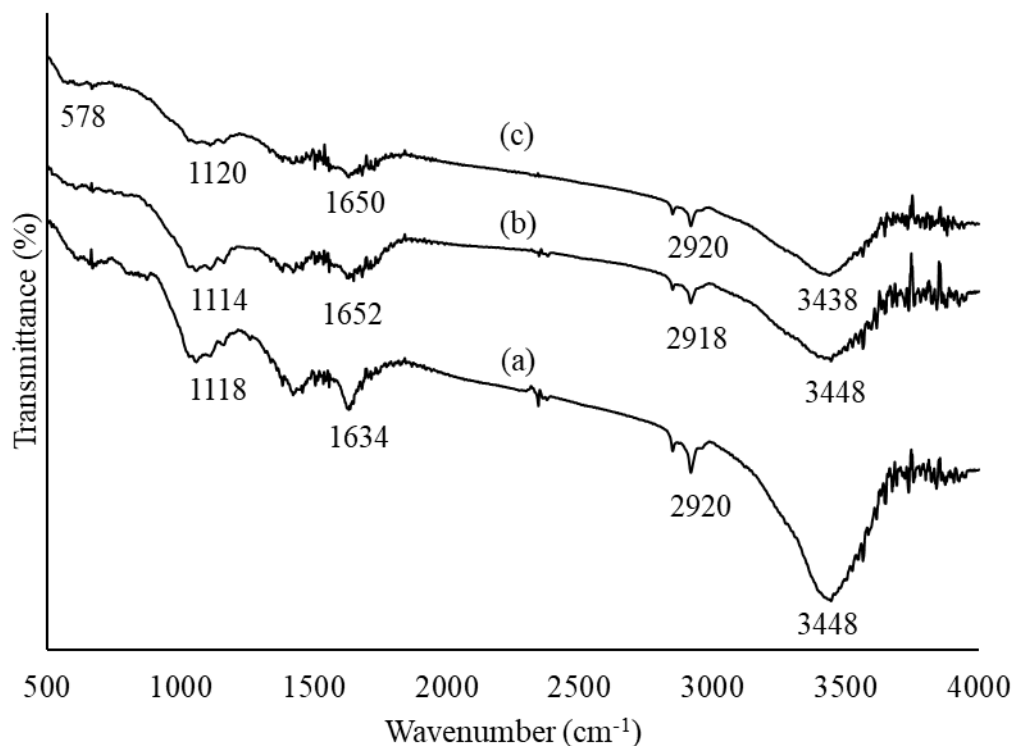
Figure 4.1: FTIR Spectra of (a) Pristine MWCNTs, (b) MWCNTs-COOH and (c) MWCNTs-Fe_3O_4 Nanocomposites.

Table 4.1: FTIR Spectra Characteristics of Pristine MWCNTs, MWCNTs-COOH and MWCNTs-Fe_3O_4 Nanocomposites.

IR peak	Frequency (cm^{-1})			Assignment
	Pristine MWCNTs	MWCNTs-COOH	MWCNTs-Fe_3O_4	
1	-	-	578	Fe-O-Fe stretching
2	1074	1030	1030	-C-C- group
3	1118	1114	1120	C-O stretching
4	1446	1426	1430	C-H bending
5	1634	1652	1650	C=C stretching
6	2920	2918	2920	C-H stretching
7	3448	3448	3438	-OH group

The presence of the significant bands in the three of the MWCNTs samples at wavenumber of about 3440 cm^{-1} were attributed to the "-OH" stretching of hydroxyl groups, which indicated the presence of moisture in the pristine MWCNTs (Gonzalez-Dominguez, et al., 2012; Malekia, et al., 2017) and the presence of -COOH groups after the acid treatment, while the bands at wavenumber of about 1650 cm^{-1} were contributed by the "C=C" stretching of aromatic rings in MWCNTs. The reduction of "C=C" and "-OH" peak intensities of MWCNTs-Fe_3O_4 nanocomposites as compared to those of MWCNTs-COOH implied that the functional group of MWCNTs might be involved in the assembling of Fe_3O_4 nanoparticles. Besides, the peaks at around 2920 cm^{-1} were associated with the "C-H" stretching of the non-ionic carboxyl groups. However, these peaks were artefacts possibly due to the hydrocarbon contamination of the optical parts of the equipment operated (Pacheco, et al., 2015).

Moving forward, the peaks at about 1430 cm^{-1} were assigned to the "C-H" bending of methyl and phenyl alcohol. The vibration bands at about 1118 cm^{-1} and 1030 cm^{-1} indicated that MWCNTs structure were also made up of the "-C-C-" groups and the "C-O" stretching of ether groups. It was reported by Huang, Yu and Jiang (2014) that an intense band around 577 cm^{-1} was attributed to "Fe-O-Fe" stretching, owing to the loading of Fe_3O_4 nanoparticles in the

MWCNTs-Fe$_3$O$_4$ nanocomposites. According to the result in this study, the small peak at 578 cm^{-1} affirmed the "Fe-O-Fe" stretching in MWCNTs-Fe$_3$O$_4$ nanocomposites. The presence of Fe$_3$O$_4$ nanoparticles in MWCNTs-Fe$_3$O$_4$ nanocomposites was further confirmed by XRD and SEM-EDX characterizations.

4.1.2   XRD Analysis

Figure 4.2 showed the XRD patterns of the pristine MWCNTs, MWCNTs-COOH, Fe$_3$O$_4$ nanoparticles and MWCNTs-Fe$_3$O$_4$ nanocomposites. It can be clearly seen that three of the MWCNTs samples had the same diffraction peaks at approximately 2θ = 26.0º that belonged to MWCNTs (Hernandez, et al., 2015). This means that the MWCNT structures of the MWCNTs-COOH and MWCNTs-Fe$_3$O$_4$ nanocomposites were not destroyed neither by the treatment of nitric acid nor the loading of Fe$_3$O$_4$ nanoparticles. The peak at 2θ = 25.92º also pertained to the index of (0 0 2), indicating the hexagonal graphite structure of MWCNTs.
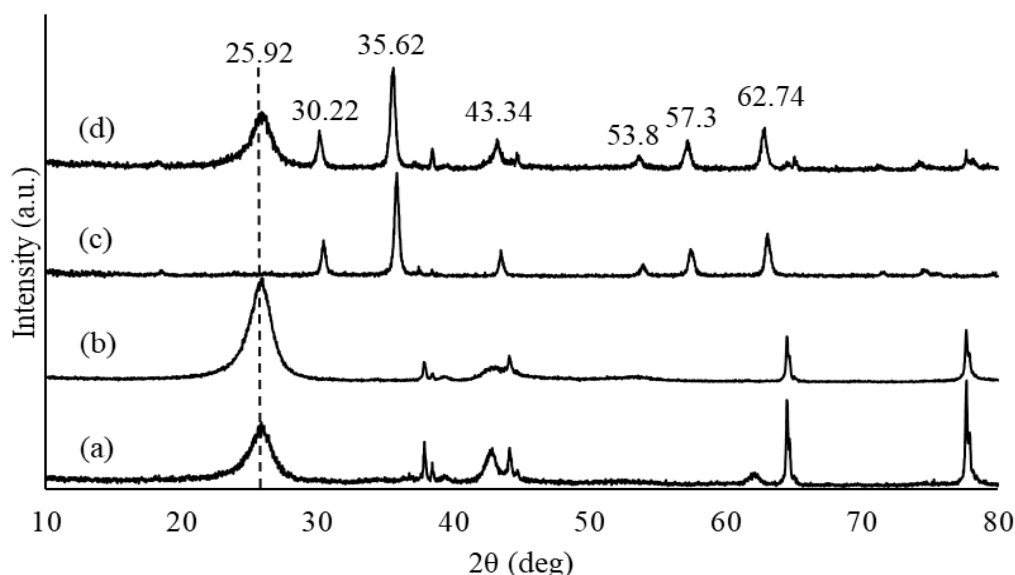
Figure 4.2: XRD Patterns of (a) Pristine MWCNTs, (b) MWCNTs-COOH, (c) Fe$_3$O$_4$ Nanoparticles and (d) MWCNTs-Fe$_3$O$_4$ Nanocomposites.

On top of that, it was observed that the MWCNTs-Fe$_3$O$_4$ nanocomposites (Figure 4.2 (d)) contained the six characteristic peaks: 2θ = 30.22º, 35.62º, 43.34º, 53.8º, 57.3º and 62.74º similar to the XRD patterns of

Fe$_3$O$_4$ nanoparticles (Figure 4.2 (c)). This proved that the MWCNTs-Fe$_3$O$_4$ nanocomposites were synthesized successfully by direct doping method. According to Song, et al. (2011), these six peaks (30.22º, 35.62º, 43.34º, 53.8º, 57.3º and 62.74º) were corresponded to the crystal planes (2 2 0), (3 1 1), (4 0 0), (4 2 2), (5 1 1) and (4 4 0), indicating that the Fe$_3$O$_4$ nanoparticles possess an inverse spinel structure.

4.1.3   SEM-EDX Analysis

The SEM images of the pristine MWCNTs, MWCNTs-COOH and MWCNTs-Fe$_3$O$_4$ nanocomposites were shown in Figure 4.3 (a), (b) and (c) respectively. Figure 4.3 (a), (b) and (c) demonstrated the hexagonal graphite structure of the MWCNTs. It can be clearly seen that the graphite structures did not have obvious change after the acid treatment and direct doping process, indicating the feasibility of using HNO$_3$ oxidation followed by solvent free direct doping method in the synthesis of MWCNTs-Fe$_3$O$_4$ nanocomposites.

Additionally, it can be observed that the MWCNTs in Figure 4.3 (a) formed bundles of tubular shape owing to the strong Van der Waals attractions (Huang, Yu and Jiang, 2014). Meanwhile, it was observed that in Figure 4.3 (c), there were clusters of Fe$_3$O$_4$ nanoparticles that adhered together and accumulated in spherical shapes as a result of the magnetostatics coupling between the particles, which were in accordance with the results reported by Rahmawati, et al. (2017). Hence, it can be clarified that Fe$_3$O$_4$ nanoparticles were successfully doped on the surface of MWCNTs.
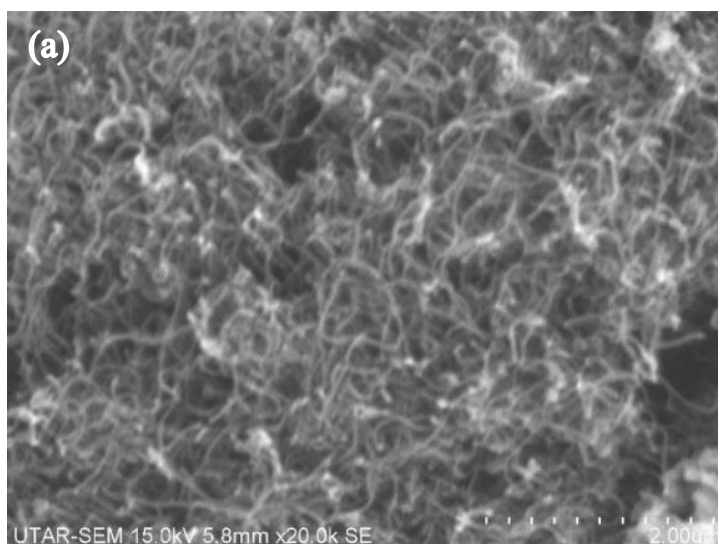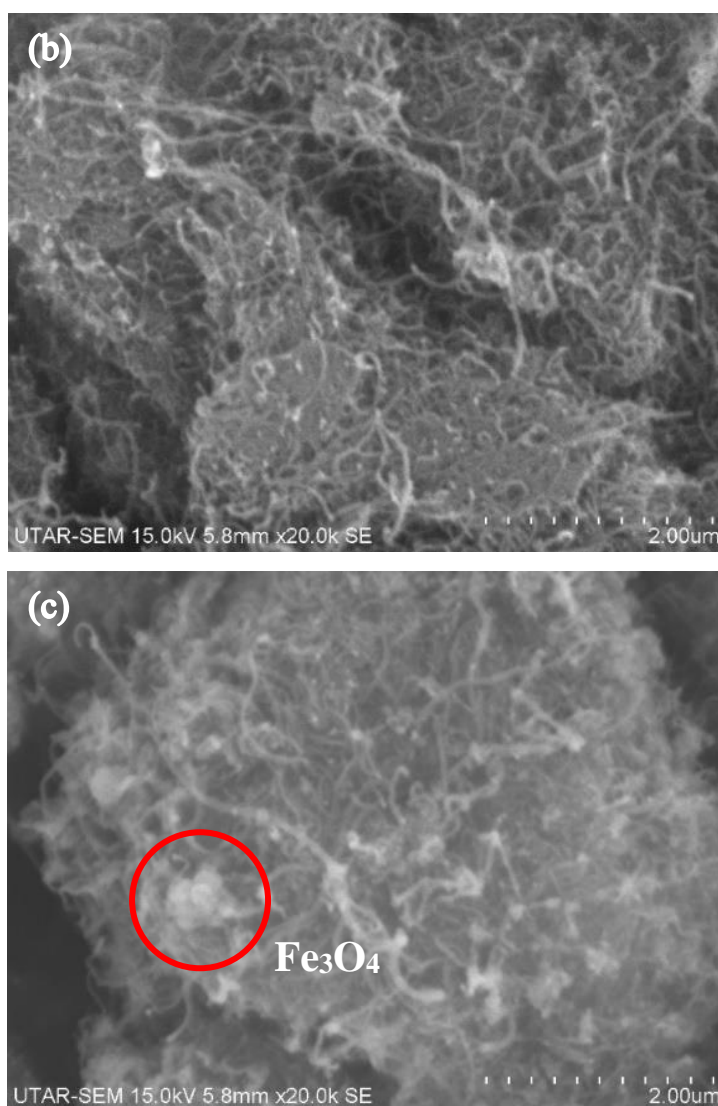
Figure 4.3: SEM Images of (a) Pristine MWCNTs, (b) MWCNTs-COOH and (c) MWCNTs-Fe$_3$O$_4$ Nanocomposites.

EDX characterization was performed and the typical EDX spectra were illustrated in Figure 4.4. The appearance of Mg signals in pristine MWCNTs and MWCNTs-COOH were determined to be 19.03 % and 0.35 % respectively, indicating that the Mg element as impurity was successfully removed during the acid treatment process. It was interesting to note that no element of Fe can be found in the MWCNTs sample prior to solvent free direct doping process. Element of Fe appeared only after the doping process as shown in Figure 4.4 (c). The presence of Fe signal (45.03 %) in MWCNTs-Fe$_3$O$_4$ nanocomposites proven that Fe$_3$O$_4$ nanoparticles had been successfully decorated on the surface of MWCNTs. The results were in line with the results of XRD and SEM analysis.
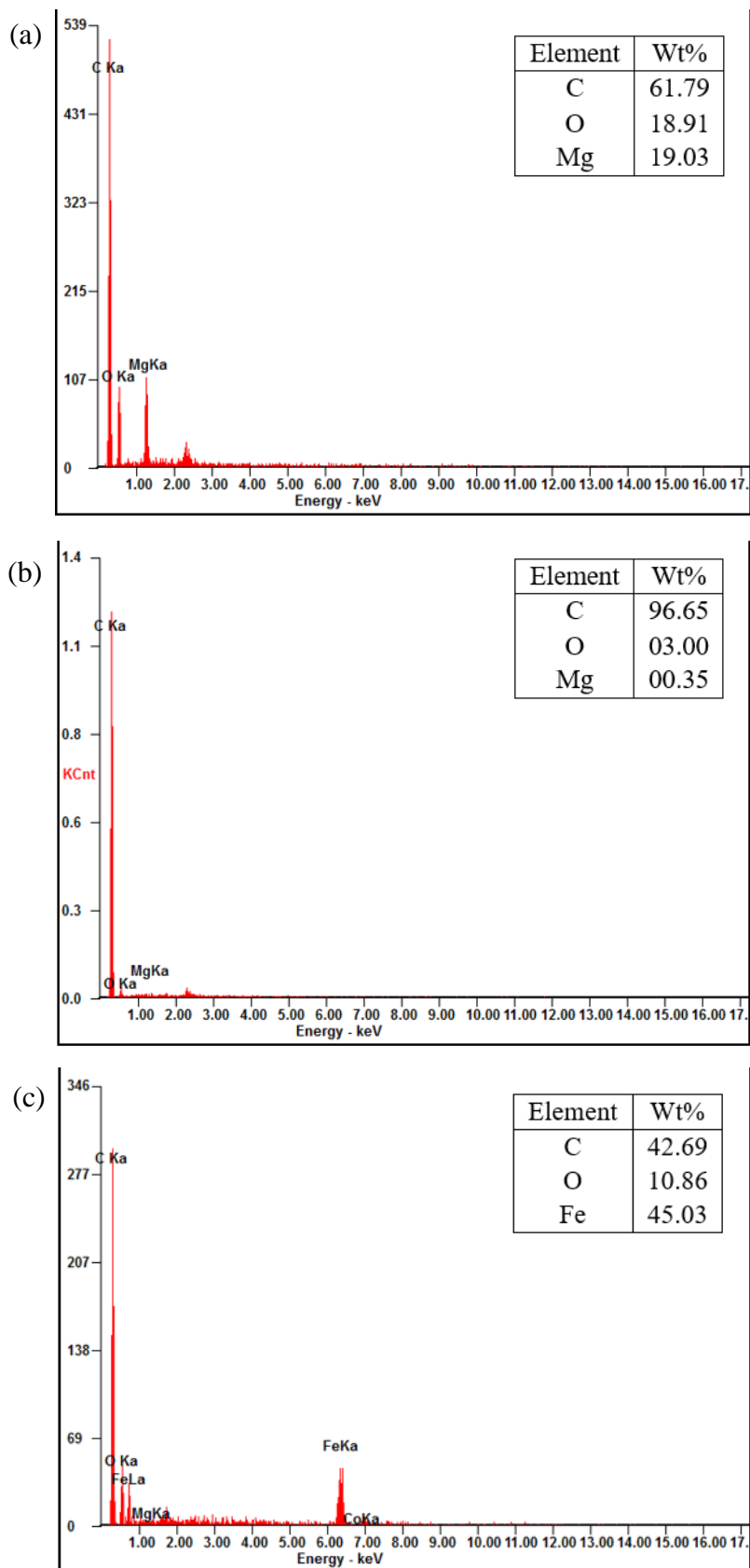
Figure 4.4: EDX Spectra of (a) Pristine MWCNTs, (b) MWCNTs-COOH and (c) MWCNTs-Fe_3O_4 Nanocomposites.

4.1.4   BET Analysis

The pore structures of pristine MWCNTs, MWCNTs-COOH and MWCNTs-Fe_3O_4 nanocomposites analysed by BET equation were presented in Table 4.2. As can be seen from the table, the MWCNTs samples were belonged to Type IV isotherm, which consisted of both micropores (diameter < 2 nm) and mesopores (2-50 nm) structures. The MWCNTs samples with the highest total BET surface area in ascending order is pristine MWCNTs, MWCNTs-COOH and MWCNTs-Fe_3O_4 nanocomposites. After acid treatment, the total BET surface area of MWCNTs-COOH increased to 157.94 m^2/g as compared to pristine MWCNTs (123.78 m^2/g). The increasing BET surface area of MWCNTs-COOH was caused by the removal of metal impurities (Birch, et al., 2013) and the repulsion force of the carboxylic groups (-COOH) grafted on the surface of MWCNTs after acid treatment, causing the debundling of MWCNTs. Furthermore, the total BET surface area of MWCNTs-Fe_3O_4 nanocomposites increased significantly 36.4 % to 168.88 m^2/g as compared to pristine MWCNTs due to the existence of Fe_3O_4 nanoparticles in the nanocomposites (Madrakian, et al., 2011).

Table 4.2: Pore Structures of Pristine MWCNTs, MWCNTs-COOH and MWCNTs-Fe_3O_4 Nanocomposites.

Sample	BET Surface Area (m^2/g)	Micropore Volume (cm^3/g)	Mesopore Volume (cm^3/g)	Total Pore Volume (cm^3/g)	Pore Diameter (nm)
Pristine MWCNTs	123.78	0.025	0.525	0.55	17.63
MWCNTs-COOH	157.94	0.017	1.293	1.31	33.14
MWCNTs-Fe_3O_4	168.88	0.012	1.238	1.25	29.66

Additionally, the MWCNTs-COOH had larger pore volume and average pore diameter than the pristine MWCNTs as the acid ultrasonication treatment had opened tube ends and created the sidewall defects on the surface of

MWCNTs (Birch, et al., 2013; Niu, et al., 2007). However, the pore volume and average pore diameter of MWCNTs-Fe_3O_4 nanocomposites were slightly lower than MWCNTs-COOH due to the attachment of Fe_3O_4 nanoparticles onto the MWCNTs, thus covering the pores of MWCNTs. Based on Arias, et al. (1999), the molecular size of methylene blue was 1.7 x 0.76 x 0.33 nm. This indicated that the average pore diameter of MWCNTs-Fe_3O_4 nanocomposites that is 29.66 nm was considered large enough for the adsorption of methylene blue.

The pore structures of MWCNTs-Fe_3O_4 nanocomposites that synthesized by chemical method reported by Mishra and Ramaprabhu (2011) and the pore structures of MWCNTs-Fe_3O_4 nanocomposites that synthesized by direct doping method in this study were compared and summarized in Table 4.3. The results showed that the BET surface area, pore volume and average pore diameter of MWCNTs-Fe_3O_4 nanocomposites that synthesized by direct doping method were higher as compared to the one synthesized by chemical method, indicating that the solvent free direct doping method was highly feasible in the synthesizing of MWCNTs-Fe_3O_4 nanocomposites.

Table 4.3: Pore Structures of MWCNTs-Fe_3O_4 Nanocomposites that Synthesized by Direct Doping Method and Chemical Method (Mishra and Ramaprabhu, 2011).

MWCNTs-Fe_3O_4	BET surface area (m^2/g)	Total Pore Volume (cm^3/g)	Pore diameter (nm)
Direct Doping	168.88	1.25	29.66
Chemical Method	70.09	0.23	12.00

4.1.5   TGA Analysis

The TGA curves for MWCNTs-COOH and MWCNTs-Fe_3O_4 nanocomposites were shown in Figure 4.5. It can be observed both MWCNTs-COOH and MWCNTs-Fe_3O_4 nanocomposites were stable up to 800 ºC. The slight weight loss of both MWCNTs samples exhibited at the temperature less than 800 ºC was due to the removal of adsorbed moisture (Sadegh, Shahryari-ghoshekandi and Kazemi, 2014). As shown in Figure 4.5 (b), a sharp weight loss was observed at temperature around 820 ºC for MWCNTs-COOH, indicating the thermal decomposition of MWCNTs-COOH. On the other hand, the thermal

decomposition of MWCNTs-Fe_3O_4 nanocomposites was extend to 850 ºC, showing that the thermal stability of MWCNTs-Fe_3O_4 nanocomposites was increased after doping of Fe_3O_4 nanoparticles. Moreover, the final weight percent of MWCNTs-Fe_3O_4 nanocomposites was found to be 27.98 %, which was higher than the final weight percent of MWCNTs-COOH that is 16.92 %. This was due to the presence of Fe_3O_4 nanoparticles in the MWCNTs-Fe_3O_4 nanocomposites.
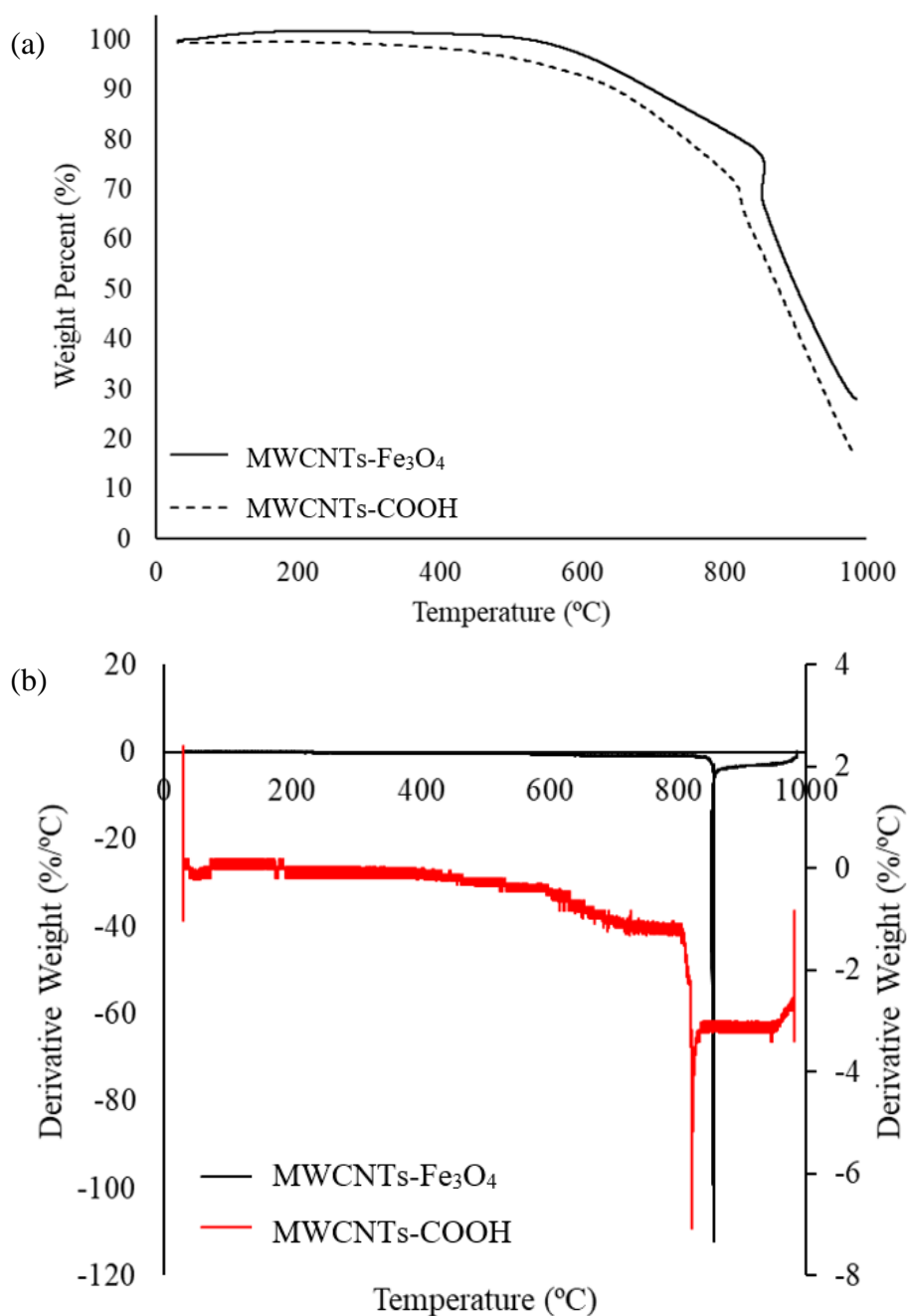
Figure 4.5: TGA Analysis of (a) Weight Percent and (b) Derivative Weight of MWCNTs-COOH and MWCNTs-Fe_3O_4 Nanocomposites.

4.2 Design Expert Simulation

4.2.1 Development of Regression Model

The percentage of adsorption and degradation of MB that affected by various process parameters were tabulated in Table 4.4. By virtue of statistical result, the percentage of adsorption and degradation were correlated to the process parameters by using regression analysis through a quadratic. Both the percentage of adsorption and degradation were then analyzed by the analysis of variance (ANOVA) and were presented in Table 4.5 and 4.6 respectively. By excluding the trivial parameters (prob > F > 0.05), the following quadratic model equations (in coded factors) that correlates the percentage of adsorption and degradation to the various process parameters were obtained.

$$\text{Percentage of Adsorption (\%)} = 7.55 + 2.74A + 2.19B - 5.17C - 1.80D - 1.98AC - 2.52BD + 1.91A^2 + 2.46B^2 \tag{4.1}$$

$$\text{Percentage of Degradation (\%)} = 92.27 - 2.85A - 2.24B + 5.88C + 1.88D + 2.25AC + 2.83BD - 1.96A^2 - 2.56B^2 \tag{4.2}$$

where

A   = pH

B   = initial MB concentration (mg/L)

C   = MWCNTs-Fe_3O_4 nanocomposites dosage (mg)

D   = H_2O_2 concentration (mmol/L)

According to the results shown in Table 4.5 and 4.6, it can be observed that the Fisher test on equation 4.1 and 4.2 gave the F-values of 11.48 and 10.71 accordingly. Both of the prob > F values were shown to be < 0.0001, indicating that the developed models were significant. Moreover, the R^2 values in both tables were 0.9146 and 0.9090, which were close to unity, suggesting that the developed models were successfully described the relationship between the process parameters and the percentage of adsorption and degradation of MB.

Table 4.4: Experiment Matrix with Coded Factors of CCD and Response.

Run	A: pH	B: Initial MB Concentration (mg/L)	C: MWCNTs-Fe_3O_4 Nanocomposites Dosage (mg)	D: H_2O_2 Concentration (mmol/L)	Percentage of Adsorption (%)	Percentage of Degradation (%)
1	6	50	20	12.50	24.31	75.38
2	4	20	15	8.75	10.50	89.20
3	4	20	25	8.75	5.09	94.45
4	4	40	25	16.25	1.93	98.03
5	6	30	20	5.00	9.00	90.90
6	4	40	15	8.75	22.23	77.61
7	8	20	15	8.75	20.70	79.15
8	6	30	10	12.50	21.61	77.90
9	8	40	15	16.25	16.20	83.61
10	8	40	15	8.75	32.06	64.08
11	8	20	25	8.75	5.40	94.55
12	4	40	15	16.25	13.68	86.16
13	6	10	20	12.50	11.88	87.54
14	2	30	20	12.50	10.80	89.04

Table 4.4 (Continued)

15	8	40	25	16.25	6.21	93.44
16	8	20	25	16.25	4.91	94.92
17	4	40	25	8.75	10.49	89.41
18	6	30	20	20.00	4.93	94.79
19	6	30	30	12.50	4.83	95.03
20	8	20	15	16.25	26.16	73.49
21	10	30	20	12.50	21.01	78.73
22	4	20	15	16.25	10.17	89.27
23	4	20	25	16.25	3.11	95.73
24	8	40	25	8.75	10.97	88.88
Repeated experiments						
25	6	30	20	12.50	3.33	96.65
26	6	30	20	12.50	8.35	91.53
27	6	30	20	12.50	10.78	88.98
28	6	30	20	12.50	8.16	91.58
29	6	30	20	12.50	8.97	90.90
30	6	30	20	12.50	5.73	94.00

Table 4.5: ANOVA for Response Surface Quadratic Model of Percentage of Adsorption.

Source	Sum of Squares	DF	Mean Square	F-value	Prob > F
Model	1607.09	14	114.79	11.48	< 0.0001 [a]
A	180.52	1	180.52	18.05	0.0007 [a]
B	115.25	1	115.25	11.53	0.0040 [a]
C	783.85	1	783.85	78.40	< 0.0001 [a]
D	77.77	1	77.77	7.78	0.0138 [a]
A²	100.23	1	100.23	10.02	0.0064 [a]
B²	165.92	1	165.92	16.59	0.0010 [a]
C²	42.20	1	42.20	4.22	0.0578 [b]
D²	2.87	1	2.87	0.2875	0.5997 [b]
AB	7.81	1	7.81	0.7808	0.3908 [b]
AC	62.73	1	62.73	6.27	0.0243 [a]
AD	0.8907	1	0.8907	0.0891	0.7694 [b]
BC	1.94	1	1.94	0.1940	0.6659 [b]
BD	101.95	1	101.95	10.20	0.0060 [a]
CD	0.7742	1	0.7742	0.0774	0.7846 [b]
Residual	149.98	15	10.00		

$R^2 = 0.9146$; Adjusted $R^2 = 0.8350$; Predicted $R^2 = 0.5932$; Standard Deviation = 3.16; Mean = 11.78

[a] Significant at 95% confident interval. [b] Not significant at 95% confident interval.

Table 4.6: ANOVA for Response Surface Quadratic Model of Percentage of Degradation.

Source	Sum of Squares	DF	Mean Square	F-value	Prob > F
Model	1742.41	14	124.46	10.71	< 0.0001 [a]
A	194.68	1	194.68	16.75	0.0010 [a]
B	120.79	1	120.79	10.39	0.0057 [a]
C	829.52	1	829.52	71.37	< 0.0001 [a]
D	84.83	1	84.83	7.30	0.0164 [a]
A²	105.14	1	105.14	9.05	0.0088 [a]
B²	180.26	1	180.26	15.51	0.0013 [a]
C²	47.42	1	47.42	4.08	0.0616 [b]
D²	2.19	1	2.19	0.1880	0.6707 [b]
AB	1.79	1	1.79	0.1543	0.7000 [b]
AC	81.35	1	81.35	7.00	0.0184 [a]
AD	0.0052	1	0.0052	0.0004	0.9835 [b]
BC	5.97	1	5.97	0.5133	0.4847 [b]
BD	127.71	1	127.71	10.99	0.0047 [a]
CD	3.65	1	3.65	0.3140	0.5835 [b]
Residual	174.34	15	11.62		

$R^2 = 0.9090$; Adjusted $R^2 = 0.8242$; Predicted $R^2 = 0.5569$; Standard Deviation = 3.41; Mean = 87.83

[a] Significant at 95% confident interval. [b] Not significant at 95% confident interval.

4.2.2   Effect of Single Process Parameter

It can be seen from Table 4.5 and 4.6 that all the four process parameters studied: pH, initial MB concentration, MWCNTs-Fe$_3$O$_4$ nanocomposites dosage and H$_2$O$_2$ concentration, were found to significantly affect the percentage of adsorption and degradation of MB as their prob > F values were less than 0.05. Since higher F value indicated the process parameter had more significant effect, thus it was observed from Table 4.5 and 4.6, the parameter that affected the percentage of adsorption and degradation of MB most significantly in ascending order was H$_2$O$_2$ concentration, initial MB concentration, pH, and lastly MWCNTs-Fe$_3$O$_4$ nanocomposites dosage.

Other than that, the positive signs for the regression coefficients in Equation (4.1) and (4.2) indicate a positive effect on the percentage of adsorption and degradation, while the negative signs indicate a negative effect. It can be seen that the pH and initial MB concentration showed a positive effect on the percentage of adsorption, whereas the MWCNTs-Fe$_3$O$_4$ nanocomposites dosage and H$_2$O$_2$ concentration showed a negative effect. In contrast, for the percentage of degradation, pH and initial MB concentration showed a negative effect while MWCNTs-Fe$_3$O$_4$ nanocomposites dosage and H$_2$O$_2$ concentration showed a positive effect. For instance, by comparing runs 9 and 10 in Table 4.4, it can be clearly seen that the percentage of degradation of MB increased significantly with higher H$_2$O$_2$ concentration. In contrast, the percentage of adsorption decreased when the H$_2$O$_2$ concentration increased.

4.2.2.1   Effect of pH

The effect of pH on the percentage of adsorption and degradation of MB was determined by using the Design Expert and illustrated in Figure 4.6 in a range of 4 to 8 with other parameters remained constant: initial MB concentration of 30 mg/L, MWCNTs-Fe$_3$O$_4$ nanocomposites dosage of 20 mg and H$_2$O$_2$ concentration of 12.5 mmol/L. As shown in Figure 4.6 (a), the percentage of adsorption increased with the increasing of pH from 4 to 8. Selen, et al. (2015) reported that the adsorption of molecules was deeply influenced by the pH of the system due to the profound influence of pH on the surface properties of the adsorbent. It was notable that the surface of the MWCNTs-Fe$_3$O$_4$

nanocomposites consisted of carboxyl groups (-COOH) and hydroxylic groups (-OH).
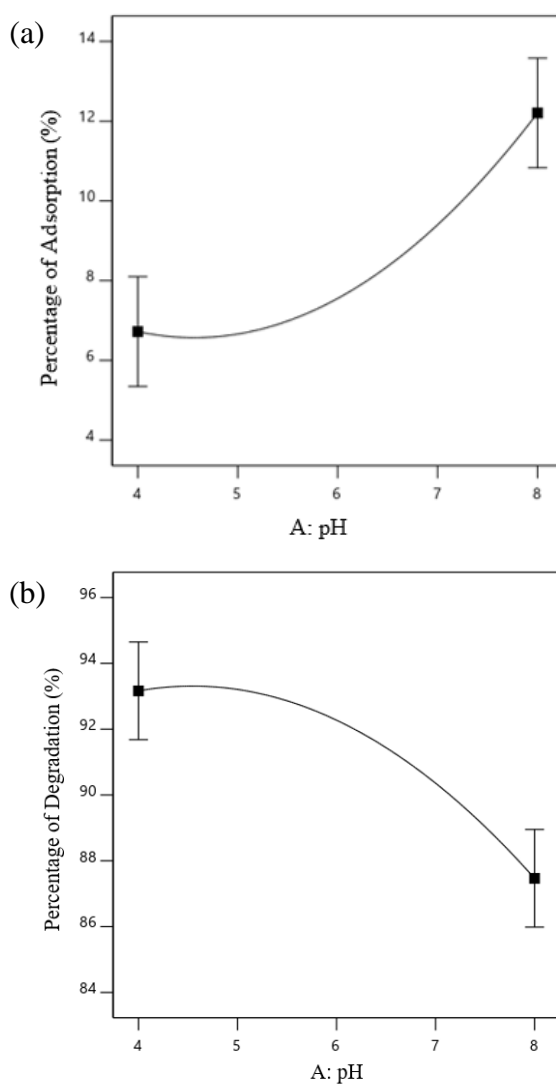
Figure 4.6: Effect of pH on Percentage of Adsorption and Degradation of MB with Initial MB Concentration = 30 mg/L, MWCNTs-Fe$_3$O$_4$ nanocomposites dosage = 20 mg and H$_2$O$_2$ concentration = 12.5 mmol/L.

At lower pH value, the adding of HCL increased the concentration of hydrogen ions (H$^+$) in the mixture by donating one of its hydrogen atoms through dissociation. This resulted in the protonation of -COOH groups on the surface of the nanocomposites as illustrated in Figure 4.7. Under these condition, the positively charged carbon atom will cause repulsion with the MB (cationic dye), resulting in a low adsorption of MB.
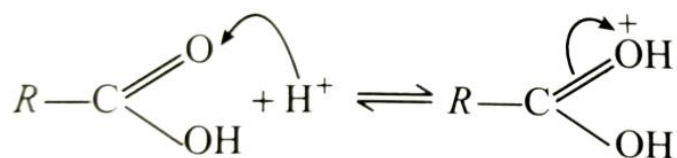
Figure 4.7: Protonation of the Carboxy Group (Doubtnut, n.d.).

On the contrary, the adding of NaOH at higher pH value increased the hydroxide ions (OH^-) in the mixture. These OH^- ions will prone to adsorb the H^+ ions in the -COOH groups on the surface of the nanocomposites. Hence, the -COOH groups will undergo dissociation into conjugate base form as shown in Figure 4.8 and the negatives charges on the surface of the nanocomposites will increase, resulting in a higher removal efficiency of MB at higher pH values (Malayeri, Sohrabi and Ghourchian, 2012).
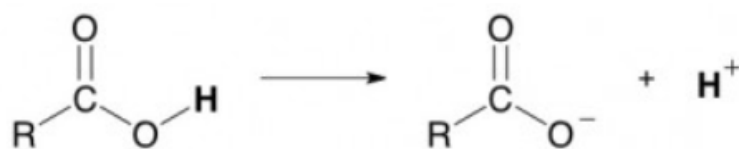
Figure 4.8: Dissociation of the Carboxy Group (Neufeldt, 2011).

However, as stated in the literature, the results carried out by Huang, Yu and Jiang (2014) and Madrakian, et.al (2011) showed that pH ranged between 6 to 7 were the best for the removal of MB. This can probably due to the increase in competition between OH^- ions and the cationic MB molecules to the limited adsorption sites on MWCNTs-Fe_3O_4 nanocomposites surface under alkaline condition. Though, the situation above did not happen in this study as pH value of 8 gave the highest percentage of adsorption of MB. This is because Fe_3O_4 nanoparticles can also serve as adsorbents for MB. Tombacz, et al. (2006) reported that at pH 8, Fe_3O_4 nanoparticles underwent deprotonation to produce FeO^- ions. These ions can adsorb the cationic MB molecules and result in a higher percentage of adsorption of MB at pH 8.

Meanwhile, from Figure 4.6 (b), high percentage of degradation was observed at pH range of 4 to 5 and decreased gradually after pH 5. The result was in good agreement with the results reported by Jiang, et al. (2011) and Fayazi, et al. (2016), which revealed that the degradation efficiency was

optimum at pH range of 3 to 5. Javaid and Qazi (2019) had stated that Fenton process was greatly dependent on the pH of the solution as it controlled the generation of •OH radicals from H_2O_2. For pH below 3, degradation efficiency will decrease owing to the formation of stable oxonium ion $[H_3O_2]^+$ that caused by the solvation of H_2O_2 under high concentration of H^+ ions. These $[H_3O_2]^+$ ions will make H_2O_2 more stable and lessen it reactivity with Fe_3O_4 nanoparticles. At pH above 5, the oxidation potential of •OH radicals were gradually restricted as they will undergo rapid conversion to their less active conjugate base, $•O^-$ (Hu, et al., 2011).

4.2.2.2   Effect of Initial MB Concentration

The effect of initial MB concentration on the percentage of adsorption and degradation of MB was determined by using the Design Expert and was shown in Figure 4.9 in a range of 10 to 50 mg/L with other parameters remained constant: pH of 6, MWCNTs-Fe_3O_4 nanocomposites dosage of 20 mg and H_2O_2 concentration of 12.5 mmol/L. It can be observed from Figure 4.9 (a) that the percentage of adsorption increased with the increase of initial MB concentration. This was because high MB concentration is vital to produce the driving force for the dyes to overcome the mass transfer resistance existed between the aqueous and solid phases. Therefore, higher initial MB concentration will enhance the percentage of adsorption (Selen, et al., 2015).

Contrarily, the result in Figure 4.9 (b) showed that higher initial MB concentration will result in lower percentage of degradation. This result was corresponded to the findings of Ahmed, et al. (2015) and Singh, et al. (2018), which stated that the increase in initial MB concentration will occupy the active sites on the catalyst surface, leading to the reduction of •OH radicals formed on the surface of MWCNTs-Fe_3O_4 nanocomposites. Besides that, the formation of FeO^- ions during the deprotonation of Fe_3O_4 nanoparticles (Tombacz, et al., 2006) can also serve as adsorbents for MB molecules. The increase in the MB molecules will however cover up the Fe_3O_4 nanoparticles, resulting in the reduction of •OH radicals formed as the H_2O_2 were unable to react with the Fe_3O_4 nanoparticles. In short, the increase number of MB molecules and insufficient concentration of •OH radicals resulted in the reduction of percentage of degradation of MB.
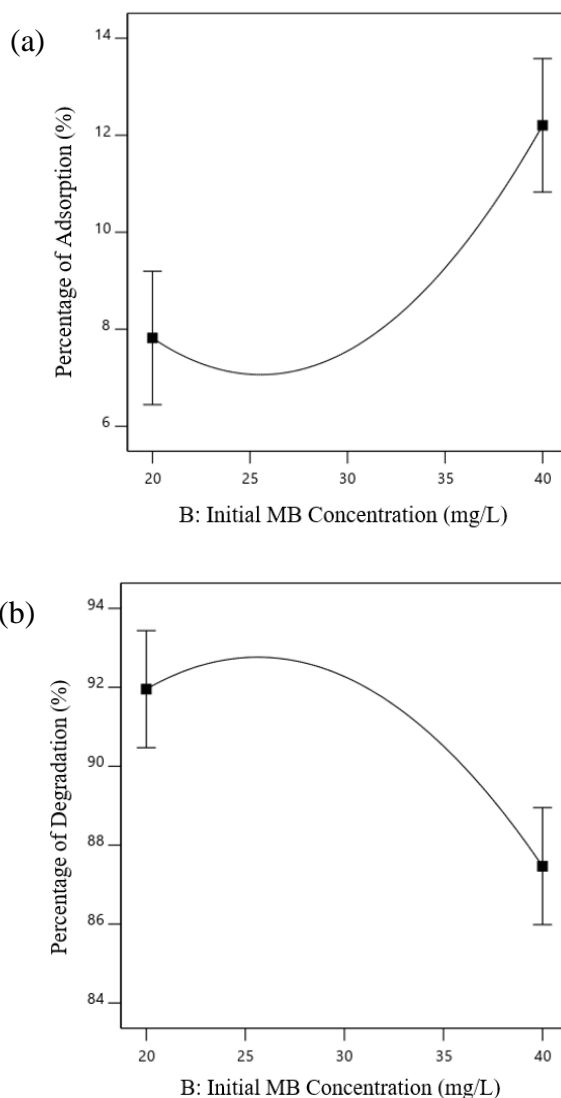
Figure 4.9: Effect of Initial MB Concentration on (a) Percentage of Adsorption and (b) Percentage of Degradation of MB with pH = 6, MWCNTs-Fe$_3$O$_4$ nanocomposites dosage = 20 mg and H$_2$O$_2$ concentration = 12.5 mmol/L.

4.2.2.3   Effect of MWCNTs-Fe$_3$O$_4$ Nanocomposites Dosage

The effect of MWCNTs-Fe$_3$O$_4$ nanocomposites dosage on the percentage of adsorption and degradation of MB was determined by using the Design Expert in a range of 10 to 30 mg with other parameters remained constant: pH of 6, initial MB concentration of 30 mg/L and H$_2$O$_2$ concentration of 12.5 mmol/L. Figure 4.10 illustrated the effect of MWCNTs-Fe$_3$O$_4$ nanocomposites dosage on the percentage of adsorption and degradation of MB. Generally, the addition of MWCNTs-Fe$_3$O$_4$ nanocomposites dosage will increase both the percentage of adsorption and degradation of MB as reported by Huang, Yu and Jiang (2014),

Hu, et al. (2011) and Jiang, et al. (2011). However, as shown in Figure 4.10 (a), the percentage of adsorption decreased with the increase of MWCNTs-Fe_3O_4 nanocomposites dosage due to the degradation of MB into water and carbon dioxide. As shown in Equation (3.4), higher percentage of degradation will automatically cause a lower percentage of adsorption. Since the percentage of degradation will increase with increasing MWCNTs-Fe_3O_4 nanocomposites dosage due to the higher number of active sites for the formation of •OH radicals (Fayazi, et al., 2016), the percentage of adsorption will therefore decrease with increasing percentage of degradation of MB.
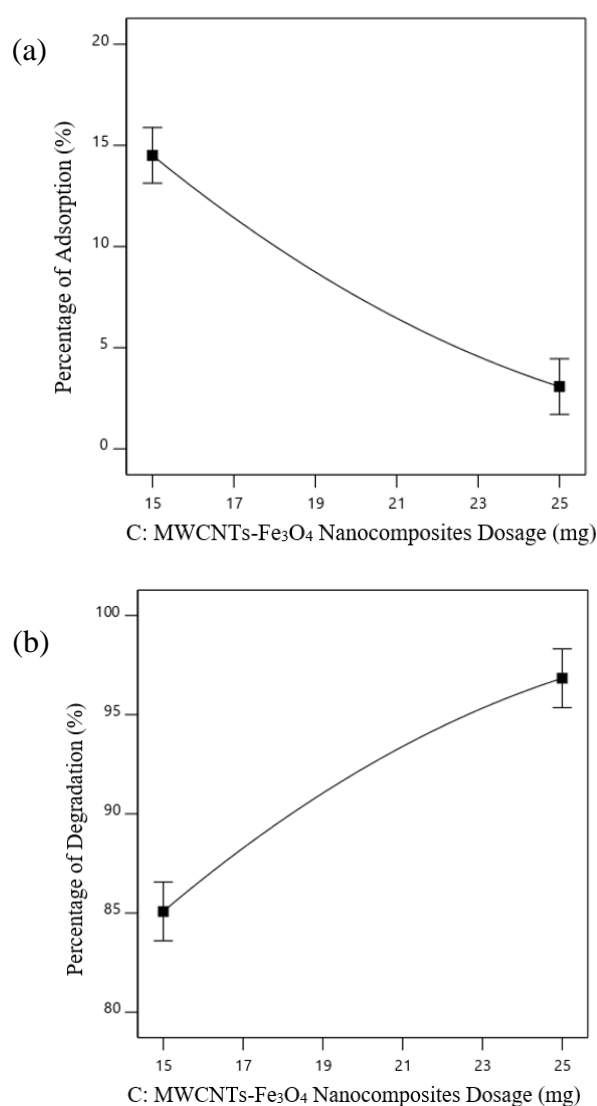
Figure 4.10: Effect of MWCNTs-Fe_3O_4 Nanocomposites Dosage on (a) Percentage of Adsorption and (b) Percentage of Degradation of MB with pH = 6, Initial MB Concentration = 30 mg/L and H_2O_2 concentration = 12.5 mmol/L.

4.2.2.4 Effect of H_2O_2 Concentration

The effect of H_2O_2 concentration on the percentage of adsorption and degradation of MB was determined by using the Design Expert in a range of 5 to 20 mmol/L with other parameters remained constant: pH of 6, initial MB concentration of 30 mg/L and MWCNTs-Fe_3O_4 nanocomposites dosage of 20 mg. However, the effect of H_2O_2 concentration on the percentage of adsorption of MB was not discussed in this study as H_2O_2 concentration had no significant effect on the adsorption of MB.

As shown in Figure 4.11, the percentage of degradation of MB was found to increase steadily with higher H_2O_2 concentration from 8.75 mmol/L to 16.25 mmol/L. Based on Fayazi, et al. (2016), the H_2O_2 concentration is a vital factor that affecting the percentage of degradation as it is directly linked to the number of •OH radicals generated in Fenton reaction. Thus, higher concentration of H_2O_2 will induce higher degradation of MB. Nonetheless, Jiang, et al. (2011) and Ahmed, et al. (2015) revealed that the concentration of H_2O_2 should not be too high as excessive H_2O_2 could cause •OH radicals scavenging effect. The scavenging effect happened when the excessive H_2O_2 competed with the MB to react with the •OH radicals to form water and •OOH radicals as shown in Equation (2.9). This scavenging effect will lead to lower percentage of degradation of MB as it will reduce the •OH radicals available for the degradation of MB. Although •OOH radicals also had the ability to mineralize MB, yet their oxidizing ability was lower than the •OH radicals and did less contribution to the degradation of MB. This scenario was however not occurred in this study as it can be seen from Figure 4.11 that the degradation of MB was most favorable in the H_2O_2 concentration of 16.25 mmol/L.
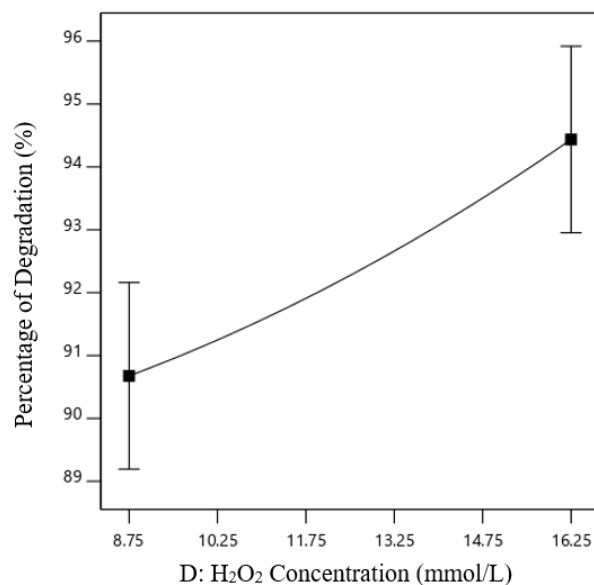
Figure 4.11: Effect of H_2O_2 Concentration on Percentage of Degradation of MB with pH = 6, Initial MB Concentration = 30 mg/L and MWCNTs-Fe_3O_4 nanocomposites dosage = 20 mg.

4.2.3 Interaction Between Parameters

The interaction between parameters was studied for the percentage of degradation of MB since it was the main focus in this study. As shown in Table 4.6, only the term AC and BD were significant at the 95 % confidence level among all the interaction terms. This meant that only interaction between pH (A) and MWCNTs-Fe_3O_4 nanocomposites dosage (C), as well as interaction between initial MB concentration (B) and H_2O_2 concentration (D) affected the percentage of degradation significantly. The two-dimensional and three-dimensional plots for the interaction between pH and MWCNTs-Fe_3O_4 nanocomposites dosage, as well as interaction between initial MB concentration and H_2O_2 concentration were shown in Figure 4.12 and 4.13 respectively.
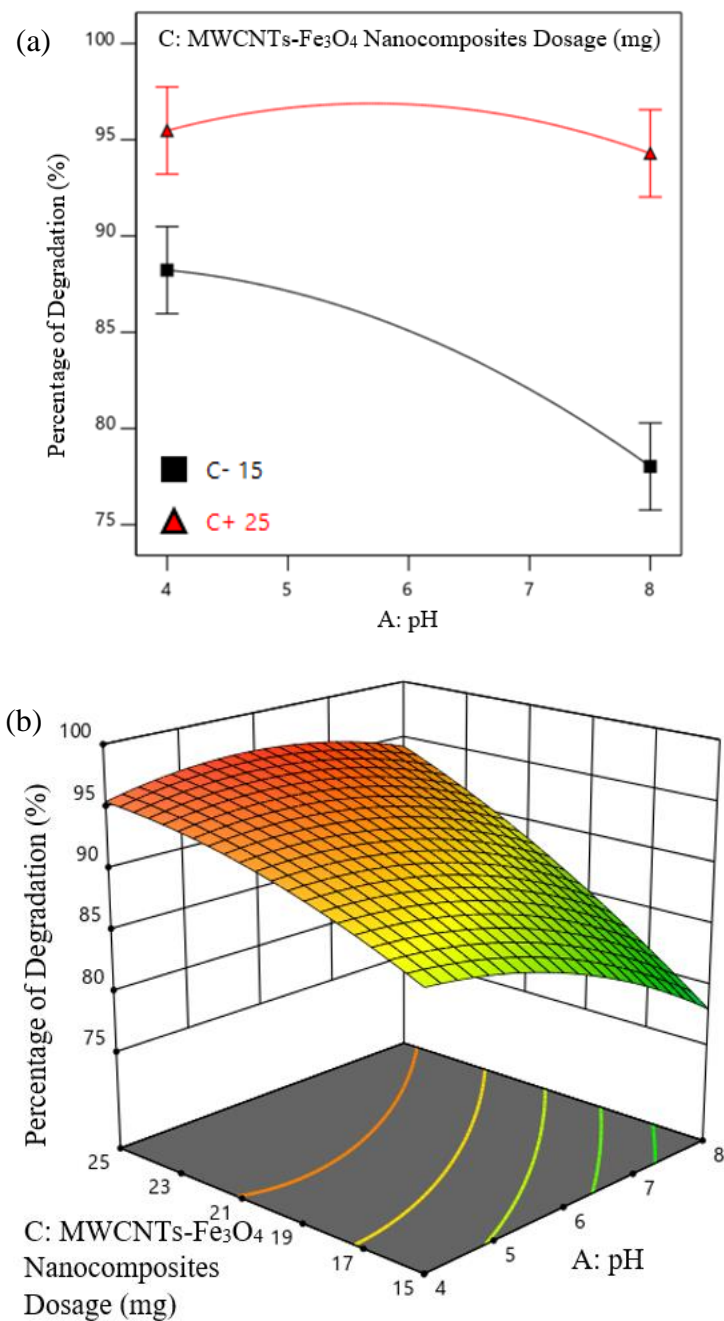
Figure 4.12: Interaction Effect between pH and MWCNTs-Fe$_3$O$_4$ Nanocomposites Dosage on Percentage of Degradation of MB: (a) Two-dimensional Plot and (b) Three-dimensional Plot.
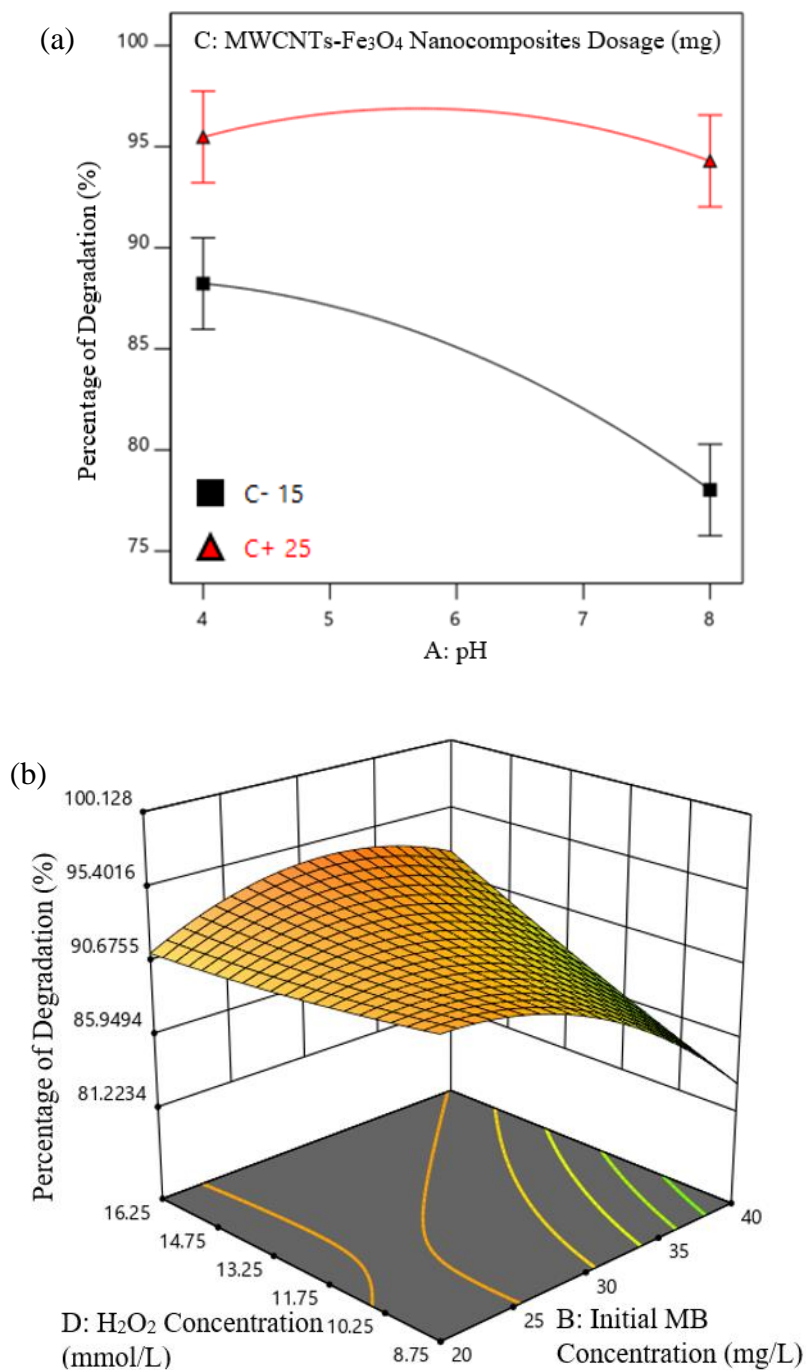
Figure 4.13: Interaction Effect between Initial MB Concentration and H_2O_2 Concentration on Percentage of Degradation of MB: (a) Two-dimensional Plot and (b) Three-dimensional Plot.

From Figure 4.12 (a), it can be observed that when the pH was set at a lower value (pH 4), the increment of MWCNTs-Fe_3O_4 nanocomposites dosage from 15 mg to 25 mg only caused a marginal increase in the percentage of degradation of MB. However, when the pH of the system was increased to

alkaline condition (pH 8), significant difference of degradation performance was observed when the MWCNTs-Fe$_3$O$_4$ nanocomposites dosage increased from 15 mg to 25 mg. It was reported that rapid decomposition of H$_2$O$_2$ occurred at high pH (Jung, et al., 2009). Therefore, lower dosage of MWCNTs-Fe$_3$O$_4$ nanocomposites at high pH (pH 8) provided less active side for the generation of •OH radicals before the decomposition of H$_2$O$_2$. Meanwhile, at 25 mg of MWCNTs-Fe$_3$O$_4$ nanocomposites loading, sufficient active sites were available for the generation of •OH radicals for the degradation of MB before H$_2$O$_2$ decomposed. This further strengthened the claim that MWCNTs-Fe$_3$O$_4$ nanocomposites dosage as the most prominent process parameters in this study.

On the other hand, it can be seen that from Figure 4.13 (a), when the initial MB concentration was set at a lower value (20 mg/L), an increase in the H$_2$O$_2$ concentration from 8.75 mmol/L to 16.25 mmol/L will cause a marginal decrease in the percentage of degradation of MB. However, when the initial MB concentration was set at a higher value (40 mg/L), the percentage of degradation of MB increased with higher H$_2$O$_2$ concentration. The phenomena above can be explained by the •OH radicals scavenging effect (Xu and Wang, 2012). At low initial MB concentration (20 mg/L), high amount of H$_2$O$_2$ (16.25 mmol/L) may lead to excessive H$_2$O$_2$, which will react with the •OH radicals to form •OOH radicals and lessening the reactive radical available for the degradation of MB. This resulted in a less amount of MB needed to compete stiffly with H$_2$O$_2$ in order to react with the •OH radicals, and thus reduced the percentage of degradation of MB. On the contrary, at high initial MB concentration (40 mg/L), low amount of H$_2$O$_2$ (8.75 mmol/L) was insufficient to generate adequate amount of •OH radicals for all the MB to degrade and therefore resulted in a lower percentage of degradation of MB. Besides, it can be observed that there is only a marginal difference of the percentage of degradation of MB when the H$_2$O$_2$ concentration increased from 8.75 mmol/L to 16.25 mmol/L. This further proved the claim that H$_2$O$_2$ concentration is the least significant process parameters in this study, which was preferable as high percentage of degradation of MB can be obtained only with a minimum amount of H$_2$O$_2$ that is corrosive and irritant.

4.2.4   Optimization of Process Parameters

The results have demonstrated that all the process parameters identified significantly affect the percentage of adsorption and degradation of MB. Next, the highest percentage of MB degradation was aimed to be obtained by optimizing the process parameters. On top of the individual process parameter, it was important to take into account the interaction between parameters during the optimization process. To achieve the optimum percentage of degradation, the regression model that developed in Equation (4.2) was used together with the optimization function that came along with the Design Expert simulation. The ranges for each of the process parameters studied in the optimization procedure were depicted in Table 4.7. The software anticipated that an optimum percentage of degradation of 98.03 % was achieved with the following process parameters: pH of 5.86, initial MB concentration of 32.22 mg/L, MWCNTs-Fe_3O_4 nanocomposites dosage of 27 mg and H_2O_2 concentration of 13.02 mmol/L. After obtaining the predicted optimum yield through the simulation, three repeated experimental runs were carried out by using the suggested optimum condition. An average optimum yield of 95.92 % was obtained from the three repeated experiment sets. The value was very close with the predicted value with a percentage error less than 5 %. Hence, it can be concluded that the predicted optimum conditions are accurate and valid for this study.

Table 4.7: Constraints Used to Optimize Percentage of Degradation of MB.

Variable	Goal	Lower Limit	Upper Limit
A: pH	In range	2	10
B: Initial MB Concentration (mg/L)	In range	10	50
C: MWCNTs-Fe_3O_4 Nanocomposites Dosage (mg)	In range	10	30
D: H_2O_2 Concentration (mmol/L)	In range	5	20
R1: Percentage of Adsorption (%)	In range	1.93	32.06
R2: Percentage of Degradation (%)	Maximize	64.08	98.03

4.3   Spent MWCNTs-Fe₃O₄ Nanocomposites

After the adsorption and degradation experiments, the spent MWCNTs-Fe$_3$O$_4$ nanocomposites were collected by using a magnet for 30 min. After that, the collected spent MWCNTs-Fe$_3$O$_4$ nanocomposites were rinsed with ethanol and dried in an oven at 80 °C overnight. Then, the nanocomposites were grounded for XRD characterisation in a 2θ range from 10° to 80° with a scanning rate of 0.02 s^{-1}. Figure 4.14 showed the XRD patterns for the MWCNTs-Fe$_3$O$_4$ nanocomposites before and after the adsorption and degradation experiments.
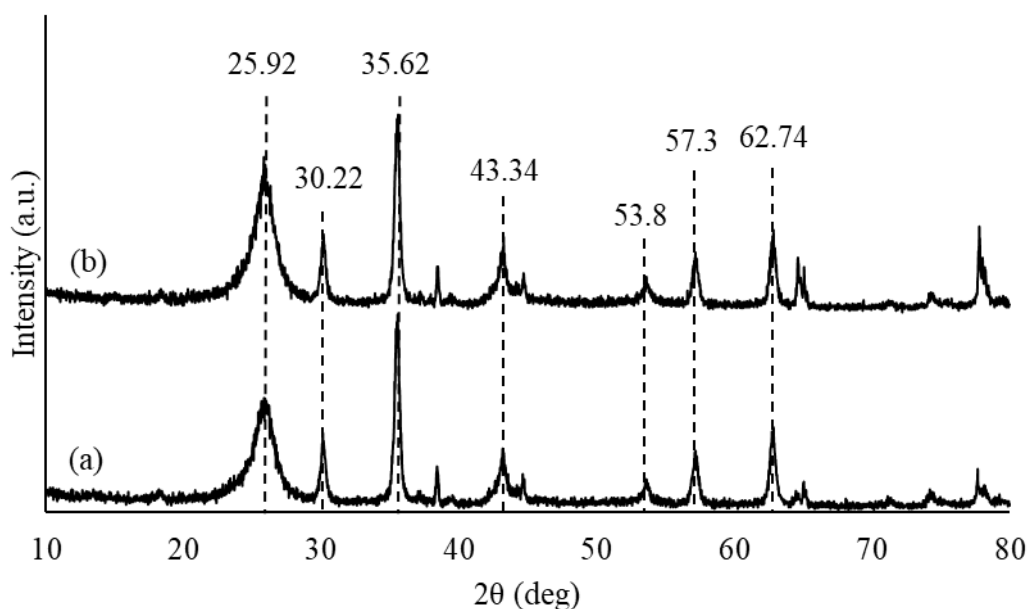
Figure 4.14: XRD Patterns of (a) MWCNTs-Fe$_3$O$_4$ Nanocomposites and (b) Spent MWCNTs-Fe$_3$O$_4$ Nanocomposites.

From Figure 4.14, it can be observed that the peaks of spent MWCNTs-Fe$_3$O$_4$ nanocomposites were relatively the same as compared to the peaks of MWCNTs-Fe$_3$O$_4$ nanocomposites. There was no other peak observed in the XRD pattern of spent MWCNTs-Fe$_3$O$_4$ nanocomposites, implying that the component and structure of the catalysts were not altered after the adsorption and degradation process. This further proved the feasibility and reusability of the MWCNTs-Fe$_3$O$_4$ nanocomposites.

CHAPTER 5

CONCLUSIONS AND RECOMMENDATIONS

5.1 Conclusions

In this study, MWCNTs-Fe$_3$O$_4$ nanocomposites were successfully prepared without using any organic reagent through a fast and convenient method: solvent free direct doping method. The synthesized catalysts were then characterized by using FTIR, XRD, SEM-EDX, BET and TGA. FTIR analysis depicted that the synthesized catalysts contained several functional groups such as "C-O", "C=C" and "C-H" stretching, as well as "-C-C-" and "-OH" groups. On top of that, "Fe-O-Fe" stretching at 578 cm^{-1} indicated the presence of Fe$_3$O$_4$ nanoparticles on the surface of the MWCNTs. Next, XRD and SEM analysis showed that synthesized catalysts consisted of both hexagonal graphite structure of MWCNTs and inverse spinel structure of Fe$_3$O$_4$ nanoparticles, while EDX characterization presented that the synthesized catalysts were mainly consisted of C, O and Fe elements. For BET analysis, it showed that the synthesized catalysts had a BET surface area of 168.88 m^2/g, total pore volume of 1.25 cm^3/g and pore diameter of 29.66 nm, which was large enough for the adsorption of MB. Lastly, TGA analysis showed that the thermal decomposition of the synthesized catalysts was around 850 ºC.

On the other hand, the effect of different process parameters: pH (2 to 10), initial MB concentration (10 to 50 mg/L), MWCNTs-Fe$_3$O$_4$ nanocomposites dosage (10 to 30 mg) and H$_2$O$_2$ concentration (5 to 20 mmol/L) on the percentage of adsorption and degradation of MB were determined by using Design Expert simulation. The results showed that higher percentage of adsorption of MB was obtained with higher pH, initial MB concentration and MWCNTs-Fe$_3$O$_4$ nanocomposites dosage. Nevertheless, in order to obtain higher percentage of degradation of MB, lower pH and initial MB concentration were needed, together with higher MWCNTs-Fe$_3$O$_4$ nanocomposites dosage and H$_2$O$_2$ concentration. By using the synthesized catalysts, it was found that with the following process parameters: pH of 5.86, initial MB concentration of 32.22 mg/L, MWCNTs-Fe$_3$O$_4$ nanocomposites dosage of 27 mg and H$_2$O$_2$

concentration of 13.02 mmol/L, an average optimum percentage of degradation of 95.92 % can be achieved. These absorption and degradation can say to be achieved high efficiency, energy saving and environmental protection for the removal of MB. In short, the MWCNTs-Fe_3O_4 nanocomposite adsorbents that consisted of commercially available high adsorption capacity of MWCNTs and separation convenience of Fe_3O_4 nanoparticles showed a satisfactory potential for the removal of MB. This method could be a potential alternative method for the removal of cationic dyes from industrial waste water.

5.2   Recommendations for Future Work

Besides the study on the effect of process parameters, kinetics study and isotherm study should be performed. The kinetics study such as pseudo-first- and pseudo-second-order kinetics will provide information about possible rate controlling step, optimum conditions and mechanism of sorption. Meanwhile, the isotherm study included Langmuir and Freundlich isotherm were also significant to evaluate the adsorption behaviour of an adsorbent.

Other than XRD, the spent MWCNTs-Fe_3O_4 nanocomposites should also be further characterized by FTIR, SEM-EDX, BET and TGA to study more on the surface structure, composites and thermal stability of the spent catalysts. Moreover, the regeneration and reusability study of spent MWCNTs-Fe_3O_4 nanocomposites should also carried out in order to assess its feasibility in practical applications.

REFERENCES

Abu-El-Halawa, R., Zabin, S. A. and Abu-Sittah, H. H., 2016. Investigation of Methylene Blue Dye Adsorption from Polluted Water Using Oleander Plant (Al Defla) Tissues as Sorbent. *American Journal of Environmental Sciences,* 12(3), pp. 213-224.

Ahmed, Y., Yaakob, Z. and Akhtar, P., 2015. Degradation and Mineralization of Methylene BLue using a Heterogenuous Photo-Fenton Catalyst under Visible and Solar Light Irradiation. *Catalyst Science & Technology,* pp. 1-32.

Ali, A., Zafar, H., Zia, M., Haq, I. u., Phull, A. R., Ali, J. S. and Hussain, A., 2016. Synthesis, characterization, applications, and challenges of iron oxide nanoparticles. *Nanotechnology Science and Applications,* 9, pp. 49-67.

Almaamary, E. A. S., Abdullah, S. R. S., Hasan, H. A., Rahim, R. A. A. and Idris, M., 2017. Treatment of Methylene Blue in Waterwater Using Scirpus Grossus. *Malaysian Journal of Analytical Sciences,* 21(1), pp. 182-187.

Al-Qodah, Z., Lafi, W. K., Al-Anber, Z., Al-Shannag, M. and Harahsheh, A., 2007. Adsorption of Methylene Blue by Acid and Heat Treated Diatomaceous Silica. *Desalination,* 217, pp. 212-224.

Anusha, G., 2013. *Chapter 3 Principles of Adsorption.* [Online] Available at: <https://shodhganga.inflibnet.ac.in/bitstream/10603/22665/8/08_chapter3.pdf> [Accessed 14 August 2019].

Arias, M., Lopez, E., Nunez, A., Rubinos, D., Soto, B., Barral, M.T. and Diaz-Fierros, F., 1999. Adsorption of Methylene Blue by Red Mud, an Oxide-Rich Byproduct of Bauxite Refining. *Effect of Mineral-Organic-Microorganism Interactions on Soil and Freshwater Environments,* pp. 361-365.

AzoNano, 2013. *Multi-Walled Carbon Nanotubes: Production, Analysis, and Application.* [Online] Available at: <https://www.azonano.com/article.aspx?ArticleID=3469> [Accessed 23 March 2020].

Berneth, H., 2008. Azine Dyes. *Ullmann's Encyclopedia of Industrial Chemistry.*

Birch, M. E., Ruda-Eberenz, T. A., Chai, M., Andrews, R. and Hatfield, R. L., 2013. Properties that Influence the Specific Surface Areas of Carbon Nanotubes and Nanofibers. *Ann Occup Hyg,* 57(9), pp. 1148-1166.

Bu, A., n.d. *Iron Oxide Nanoparticles, Characteristics and Applications.* [Online] Available at: <https://www.sigmaaldrich.com/technical-documents/articles/technology-spotlights/iron-oxide-nanoparticles-characteristics-and-applications.html> [Accessed 26 March 2020].

Buxton, R., 2007. *Design Expert 7: Introduction.* [Online] Available at: <https://www.lboro.ac.uk/media/wwwlboroacuk/content/mlsc/downloads/Design%20Expert%207.pdf> [Accessed 23 March 2020].

Carmen, Z. and Daniela, S., 2012. Textile Organic Dyes – Characteristics, Polluting Effects and Separation/Elimination Procedures from Industrial Effluents – A Critical Overview. *Organic Pollutants Ten Years After the Stockholm Convention – Environmental and Analytical Update* .

Carrara, S., 2010. Nano-Bio-Technology and Sensing Chips: New Systems for Detection in Personalized Therapies and Cell Biology. *Sensors,* 10, pp. 526-543.

Cheng, J. P., Zhang, X. B., Yi, G. F., Ye, Y. and Xia, M. S., 2008. Preparation and Magnetic Properties of Iron Oxide and Carbide Nanoparticles in Carbon Nanotube Matrix. *Journal of Alloys and Compounds,* 455, pp. 5-9.

Chunha, J. P., 2016. *Methylene Blue.* [Online] Available at: <https://www.rxlist.com/methylene-blue-side-effects-drug-center.htm#overview> [Accessed 3 July 2019].

Dawood, S. and Sen, T. K., 2014. Review on Dye Removal from Its Aqueous Solution into Alternative Cost Effective and Non-Conventional Adsorbents. *Journal of Chemical and Process Engineering.*

Doubtnut, n.d. *Explain the mechanism of esterification carboxylic acids..* [Online] Available at: <https://doubtnut.com/question-answer-chemistry/explain-the-mechanism-of-esterification-carboxylic-acids-35022228> [Accessed 14 March 2020].

Dwivedi, D. P. B., 2016. *Kinetics & Modeling of Adsorption Process.* [Online] Available at: <https://www.slideshare.net/DrPriyBratDwivedi/kinetics-modeling-of-adsorption-processpptx> [Accessed 31 July 2019].

Eljiedi, A. A. A. and Kamari, A., 2017. Removal of Methyl Orange and Methylene Blue Dyes from Aqueous Solution Using Lala Clam (Orbicularia Orbiculata) Shell.

Elmorsi, T. M., 2011. Equilibrium Isotherms and Kinetic Studies of Removal of Methylene Blue Dye by Adsorption onto Miswak Leaves as a Natural Adsorbent. *Journal of Environment Protection,* 2, pp. 817-827.

eMedicalPrep, 2019. *Adsorption.* [Online] Available at: <https://www.emedicalprep.com/study-material/chemistry/surface-chemistry/adsorption/#_Mechanism_of_Adsorption> [Accessed 14 August 2019].

EPA Victoria, 2018. *Point and Nonpoint Sources of Water Pollution.* [Online] Available at: <https://www.epa.vic.gov.au/your-environment/water/protecting-victorias-waters/point-and-nonpoint-sources-of-water-pollution> [Accessed 3 July 2019].

Fayazi, M., Taher, M. A., Afzali, D. and Mostafavi, A., 2016. Enhanced Fenton-like Degradation of Methylene Blue by Magnetically Activated Carbon/Hydrogen Peroxide with Hydroxylamine as Fenton Enhancer. *Journal of Molecular Liquids,* pp. 781-787.

Fugetsu, B., Satoh, S., Shiba, T., Mizutani, T., Lin, Y., Terui, N., Nodasaka, Y., Sasa, K., Shimizu, K., Akasaka, T., Shindoh, M., Shibata, K., Yokoyama, A., Mori, M., Tanaka, K., Sato, Y., Tohji, K., Tanaka, S., Nishi, N. and Watari, F., 2004. Caged Multiwalled Carbon Nanotubes as the Adsorbents for Affinity-Based Elimination of Ionic Dyes. *Environmental Science & Technology,* 38, pp. 6890-6896.

Ghaffar, A. and Younis, M. N., 2015. Interaction and Thermodynamics of Methylene Blue Adsorption on Oxidized Multi-walled Carbon Nanotubes. *Green Process Synth,* 4, pp. 209-217.

Gonzalez-Dominguez, J. M., Castell, P., Bespin-Gascon, S., Anson-Casaos, A., Diez-Pascual, A. M., Gomez-Fatou, M. A., Benito, A. M., Maser, W. K. and Martinez, M. T., 2012. Covalent functionalization of MWCNTs with poly(p-phenylene sulphide)oligomers: a route to the efficient integration through a chemical approach. *Jounal of Materials Chemistry,* 22, pp. 21285.

Haseena, M., Malik, M. F., Javed, A., Arshad, S., Asif, N., Zulfiqar, S. and Hanif, J., 2017. Water Pollution and Human Health.. *Environmental Risk Assessment and Remediation,* 1(3).

Hassan, A. F., Abdel-Mohsen, A. M. and Fouda, M. M. G., 2014. Comparative Study of Calcium Alginate, Activated Carbon, and Their Composite Beads on Methylene Blue Adsorption. *Carbohydrate Polymers,* 102, pp. 192-198.

Hernandez, J. S. T., Muriel, A. A., Tabares, J. A., Alcazar, G. A. P. and Bolanos, A., 2015. Preparation of Fe_3O_4 Nanoparticles and Removal of Methylene Blue through Adsorption. *Journal of Physics: Comference Series,* 614.

Huang, H., Yu, J. and Jiang, X., 2014. Preparation of Magnetic Oxidized Multiwalled Carbon Nanotubes for the Adsorption of Rhodamine B in Aqueous Solution. *Nano: Brief Reports and Reviews,* 9(8).

Hu, X., Liu, B., Deng, Y., Chen, H., Luo, S., Sun, C. and Yang, P., 2011. Adsorption and Heterogeneous Fenton Degradation of 17α-methyltestosterone on Nano Fe_3O_4/MWCNTs in Aqueous Solution. *Applied Catalyst B: Environmental,* 107(3-4), pp. 274-283.

Jasrotia, K., 2015. *Removal of Methylene Blue by Advanced Oxidation using Fenton's Reagent and Microfiltration,* Patiala: Thapar University.

Javaid, R. and Qazi, U. Y., 2019. Catalytic Oxidation Process for the Degradation of Synthetic Dyes: An Overview. *International Journal of Environmental Research and Public Health,* pp. 27.

Jiang, J., Zou, J., Zhu, L., Huang, L., Jiang, H. and Zhang, Y., 2011. Degradation of Methylene Blue with H_2O_2 Activated by Peroxidase-Like Fe_3O_4 Magnetic Nanoparticles. *Journal of Nanoscience and Nanotechnology,* 11, pp. 4793-4799.

Jung, Y. S., Lim, W. T., Park, J. Y. and Kim, Y. H., 2009. Effect of pH on Fenton and Fenton-like oxidation. *Environmental Technology,* 30(2), pp. 183-190.

Kant, R., 2012. Textile Dyeing Industry an Environmental Hazard. *Natural Science,* 4(1), pp. 23.

Karthik, R., Muthezhilan, R., Hussain, A. J., Ramalingam, K. and Rekha, V., 2015. Effective Removal of Methylene Blue Dye from Water Using Three Different Low-cost Adsorbents. *Desalination and Water Treatment,* pp. 1-6.

Li, S., He, M., Li, Z., Li, D. and Pan, Z., 2017. Removal of Humic Acid from Aqueous Solution by Magnetic Multiwalled Carbon Nanotubes Decorated with Calcium. *Journal of Molecular Liquids.*

Li, X. M., Xu, G., Liu, Y. and He, T., 2011. Magnetic Fe_3O_4 Nanoparticles: Synthesis and Application in Water Treatment. *Nanoscience and Nanotechnology-Asia,* 1(1), pp. 11.

Long, R. Q. and Yang, R. T., 2001. Carbon Nanotubes as Superior Sorbent for Dioxin Removal. *Journal of the American Chemical Society,* 123, pp. 2058-2059.

Madrakian, T., Afkhami, A., Ahmadi, M. and Bagheri, H., 2011. Removal of Some Cationic Dyes from Aqueous Solutions Using Magnetic-Modified Multi-walled Carbon Nanotubes. *Journal of Hazardous Materials,* 196, pp. 109-114.

Malayeri, F. H., Sohrabi, M. R. and Ghourchian, H., 2012. Magnetic Multi-Walled Carbon Nanotube as an Adsorbent for Toluidine Blue O Removal from Aqueous Solution. *Int. J. Nanosci. Nanotechnol.,* 8(2), pp. 79-86.

Malekia, A., Hamesadeghia, U., Daraeia, H., Hayatia, B., Najafib, F., McKayc, G. and Rezaee, R., 2017. Amine functionalized multi-walled carbon nanotubes: Single and binarysystems for high capacity dye removal. *Chemical Engineering Journal,* 313, pp. 826-835.

Mishra, A. K. and Ramaprabhu, S., 2011. Nano magnetite decorated multiwalled carbon nanotubes: a robustnanomaterial for enhanced carbon dioxide adsorption. *Energy & Environmental Science,* 4, pp. 889-895.

Nanowerk, 2019. *Carbon Nanotubes – What They Are, How They Are Made, What They Are Used For.* [Online] Available at: <https://www.nanowerk.com/nanotechnology/introduction/introduction_to_na notechnology_22.php> [Accessed 1 August 2019].

Neufeldt, S., 2011. *Sour Patch Kids are Full of Protons.* [Online] Available at: <http://icanhasscience.com/fun-stuff/sour-patch-kids-are-full-of-protons/> [Accessed 14 March 2020].

Niu, J. J., Wang, J. N., Jiang, Y., Su, L. F. and Ma, J., 2007. An Approach to Carbon Nanotubes with High Surface Area and Large Pore Volume. *Micropores and Mesopores Materials,* 100, pp. 1-5.

Pena, R. C., Silva, V. O., Quina, F. H. and Bertotti, M., 2012. Hydogen Peroxide Monitoring in Fenton Reaction by Using a Ruthenium Oxide Hexacyanoferrate/Multiwalled Cabon Nanotubes Modified Electrode. *Journal of Electroanalytical Chemistry,* 686, pp. 1-6.

Pereira, M. C., Oliveira, L. C. A. and Murad, E., 2012. Iron Oxide Catalysts: Fenton and Fenton-like Reaction. *Clay Minerals,* Volume 47, pp. 288.

Prola, L. D., Machado, F. M., Bergmann, C. P., Souza, F. E., Gally, C. R., Lima, E. C., Adebayo, M. A., Dias, S. L. P. and Calvete, T., 2013. Adsorption of Direct Blue 53 Dye from Aqueous Solutions by Multi-walled Carbon Nanotubes and Activated Carbon.. *Journal of Environmental Management,* pp. 166-175.

Rahmawati, R., Melati, A., Taufiq, A., Sunaryono, Diantoro, M., Yuliarto, B., Suyatman, S., Nugraha, N. and Kurniadi, D., 2017. Preparation of MWCNT-Fe_3O_4 Nanocomposites from Iron Sand Using Sonochemical Route. *IOP Conference Series: Materials Science and Engineering,* 202.

Rajabi, M., Mahanpoor, K. and Moradi, O., 2017. Removal of Dye Molecules from Aqueous Solution by Carbon Nanotubes and Carbon Nanotube Functional Groups: Critical Review. *RSC Advances,* 7, pp. 47083-47090.

Rashed, M. N., 2013. Adsorption Technique for the Removal of Organic Pollutants from Water and Wastewater. *Organic Pollutants - Monitoring, Risk and Treatment.*

Sadegh, H., Shahryari-ghoshekandi, R. and Kazemi, M., 2014. Study in synthesis and characterization of carbon nanotubes decorated by magnetic iron oxide nanoparticles. *International Nano Letters,* 4, pp. 129-135.

Selen, V., Guler, O., Ozer, D. and Evin, E., 2015. Synthesized Multi-walled Carbon Nanotubes as a Potential Adsorbent for the Removal of Methylene Blue Dye: Knetics, Isotherms, and Thermodynamics. *Desalination and Water Treatment,* pp. 1-13.

Sharma, M., Kalita, P., Senapati, K. K. and Garg, A., 2018. Study on Magnetic Materials for Removal of Water Pollutants. *Emerging Pollutants-Some Strategies for the Quality Preservation of Our Environment.*

Shodhganga, 2008. *Chapter 1.* [Online] Available at: <https://shodhganga.inflibnet.ac.in/bitstream/10603/4821/8/08_chapter%201.pdf> [Accessed 14 August 2019].

Singh, J., Chang, Y. Y., Koduru, J. R. and Yang, J. K., 2018. Potential Degradation of Methylene Blue (MB) by Nano-metallic Particles: A Kinetics Study and Possible Mechanism of MB Degradation. 23(1), pp. 1-9.

Sljukic, B., Banks, C. E. and Compton, R. G., 2006. Iron Oxide Particles Are the Active Sites for Hydrogen Peroxide Sensing at Multiwalled Caron Nanotube Modified Electrodes. *Nano Letters,* 6(7), pp. 1556-1558.

Song, X., Yang, F., Wang, X. and Zhang, K., 2011. Preparation of Magnetic Carbon Nanotubes and Their Application in Active Dye Removal. *Micro & Nano Letters,* 6(10), pp. 827-829.

Stat-Ease, 2017. *Handbook for Experimenters.* [Online] Available at: <https://cdnm.statease.com/pubs/handbk_for_exp_sv.pdf> [Accessed 23 March 2020].

Stoffelbach, F. Aqil, A., Jerome, C., Jerome, R. and Detrembleur, C., 2005. An Easy and Economically Viable Route for the Decoration of Carbon Nanotubes by Magnetite Nanoparticles, and Their Orientation in Magnetic Field. *Communication,* 36, pp. 4532.

Tae, K. I. and Tannenbaum, R., 2011. Magnetic Carbon Nanotubes: Synthesis, Characterization and Anisotropic Electrical Properties. *Electronic Properties of Carbon Nanotubes.*

Techinstro, 2018. *Difference between Single-walled Carbon Nanotubes and Multi-walled Carbon Nanotubes.* [Online] Available at: <https://www.techinstro.com/difference-between-single-walled-carbon-nanotubes-and-multi-walled-carbon-nanotubes/> [Accessed 1 August 2019].

Tombacz, E., Majzik, A., Horvat, Z. and Illes, E., 2006. Magnetite In Aqueous Medium: Coating Its Surface and Surface Coating With It. *Romanian Reports in Physics,* 58(3), pp. 281-286.

Water Education Foundation, n.d. *Point Source Vs Nonpoint Source Pollution.* [Online] Available at: <https://www.watereducation.org/aquapedia-background/point-source-vs-nonpoint-source-pollution> [Accessed 3 July 2019].

Xu, L. and Wang, J., 2012. Fenton- like Degradation of 2,4-dichlorophenol using Fe_3O_4 Magnetic Nanoparticles. *Applied Catalysis B: Environmental,* 123-124, pp. 117-126.

Yao, Y., He, B., Xu, F. and Chen, X., 2011. Equilibrium and Kinetic Studies of Methyl Orange Adsorption on Multiwalled Carbon Nanotubes. *Chemical Engineering Journal,* 170(1), pp. 82-89.

Zhong, Y. Li, G., Liu, S., Zhong, M., Wang, H. and Li, H., 2012. Facile Decoration and Characterization of Multi-walled Carbon Nanotubes with Magnetic Fe3O4 Nanoparticles. *Journal of Optoelectronics and Advanced Materials,* 14(3-4), pp. 245-250.

APPENDICES

APPENDIX A: Preparation of Various Concentrations of MB

Dilution method is used to obtain different MB concentration from the MB stock solution. By acknowledging the concentration of MB stock solution, as well as the concentration and volume of dilute solution, the volume of MB stock solution that needed to achieve the desired MB concentration can be calculated as follow:

$$C_1 V_1 = C_2 V_2$$

where

C_1 = concentration of stock solution, ppm

V_1 = volume of stock solution, mL

C_2 = concentration of dilute solution, ppm

V_2 = volume of dilute solution, mL

At first, 60 mg of MB powder was dissolved in 1 L of distilled water in order to obtain a MB stock solution of 60 ppm (or mg/L). Then, the sample calculation to obtain the solution with MB concentration of 10 ppm was performed by using the equation below.

$$C_1 V_1 = C_2 V_2$$
$$(60 \ ppm)V_1 = 10 \ ppm(15 \ mL)$$
$$V_1 = 2.5 \ mL$$

From the calculation, 2.5 mL of stock solution (MB solution with concentration of 60 ppm) was needed in a 15 mL final solution in order to achieve 10 ppm of MB. Therefore, 2.5 mL of MB stock solution was pipetted into a glass bottle and then added with H_2O_2 and distilled water until the mark of 15 mL. Table A-1 below showed the volume of 60 ppm MB stock solution required to prepare various concentration of MB in 15 mL solution.

Table A-1: Volume of 60 ppm MB Stock Solution Required to Prepare Various Concentration of MB in 15 mL Solution.

Concentration of MB (ppm)	Volume of 60 ppm MB Stock Solution Required (mL)
10	2.50
20	5.00
30	7.50
40	10.0
50	12.5

APPENDIX B: Preparation of Various Concentration of H_2O_2

Before the preparation of different concentration of H_2O_2, the H_2O_2 stock solution with a molar concentration of 0.1 mol/L will first be prepared by using the H_2O_2 chemical available in the laboratory with a concentration of 30 % H_2O_2 (w/w) in H_2O (30 g of H_2O_2 presented in 100 g of solution). With the knowledge on the density of 30 % H_2O_2 that is 1.11 g/mL, the volume for 100 g of 30 % H_2O_2 can be computed as below:

$$\rho = \frac{m}{V}$$

Where

ρ = density, g/mL

m = mass, g

V = volume, mL

$$V = \frac{m}{\rho}$$
$$= \frac{100 \ g}{1.11 \ \frac{g}{mL}}$$
$$= 90.09 \ mL$$

Once the volume of 100 g of 30 % H_2O_2 was calculated, the concentration of H_2O_2 abbreviated as w/v can be calculated.

$$w/v = \frac{mass \ of \ solute \ (g)}{volume \ of \ solution \ (mL)}$$
$$= \frac{30 \ g}{90.09 \ mL}$$
$$= 0.333 \ \frac{g}{mL}$$

After that, the molarity of H_2O_2 presented in 0.333 g/mL of H_2O_2 was computed by using the atomic mass of H_2O_2 that is 34.01 g/mol.

$$Molarity = \frac{0.333\ g}{mL} \times \frac{mol}{34.01\ g} \times \frac{1000\ mL}{1L}$$

$$= 9.8\ \frac{mol}{L}$$

Next, the 0.1 mol/L of H_2O_2 stock solution can be prepared from the 9.8 mol/L of H_2O_2 chemical by using the dilution method.

$$C_1V_1 = C_2V_2$$

$$\left(9.8\ \frac{mol}{L}\right)V_1 = 0.1\ \frac{mol}{L}(100\ mL)$$

$$V_1 = 1.02\ mL$$

Thus, to prepare the 0.1 mol/L of H_2O_2 stock solution with a volume of 100 mL, 1.02 mL of 9.8 mol/L of H_2O_2 chemical need to be pipetted and mixed with 98.98 mL of distilled water.

After the H_2O_2 stock solution was prepared, different concentration of H_2O_2 can be obtained from the stock solution by using dilution method. The volume of H_2O_2 stock solution that required to prepare 15 mL of solution with H_2O_2 concentration of 5 mmol/L was shown in below:

$$C_1V_1 = C_2V_2$$

$$\left(0.1\ \frac{mol}{L}\right)V_1 = 0.005\ \frac{mol}{L}(15\ mL)$$

$$V_1 = 0.75\ mL$$

From the calculation, 0.75 mL of 0.1 mol/L H_2O_2 stock solution was pipetted to a glass bottle before the adding of MB and distilled water to achieve 15 mL of solution with H_2O_2 concentration of 5 mmol/L. Table B-1 below showed the volume of 0.1 mol/L H_2O_2 stock solution required to prepare various concentration of H_2O_2 in 15 mL solution.

Table B-1: Volume of 0.1 mol/L H_2O_2 Stock Solution Required to Prepare Various Concentration of H_2O_2 in 15 mL Solution.

Concentration of H_2O_2 (mmol/L)	Volume of 0.1 mol/L H_2O_2 Stock Solution Required (mL)
5.000	0.750
8.750	1.313
12.50	1.875
16.25	2.438
20.00	3.000

APPENDIX C: Standard Calibration Curves for MB
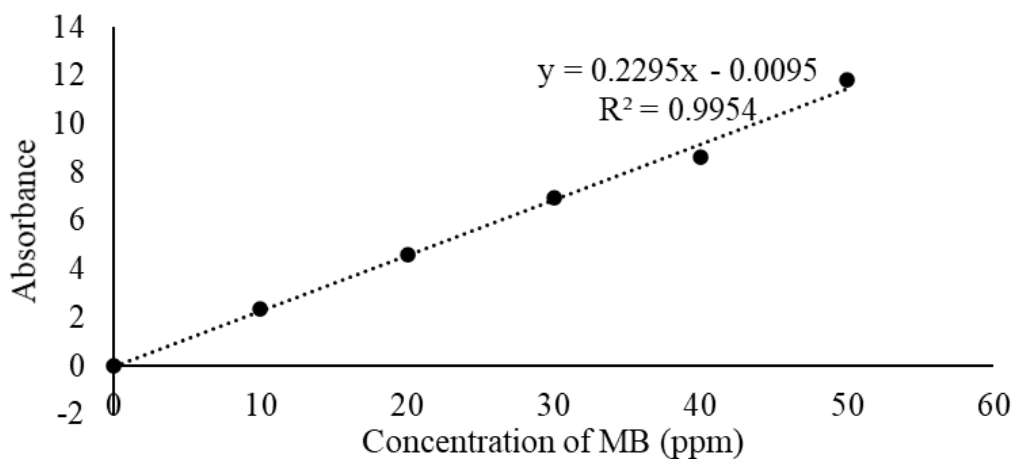
Figure D-1: Standard Calibration Curve for MB in Distilled Water.
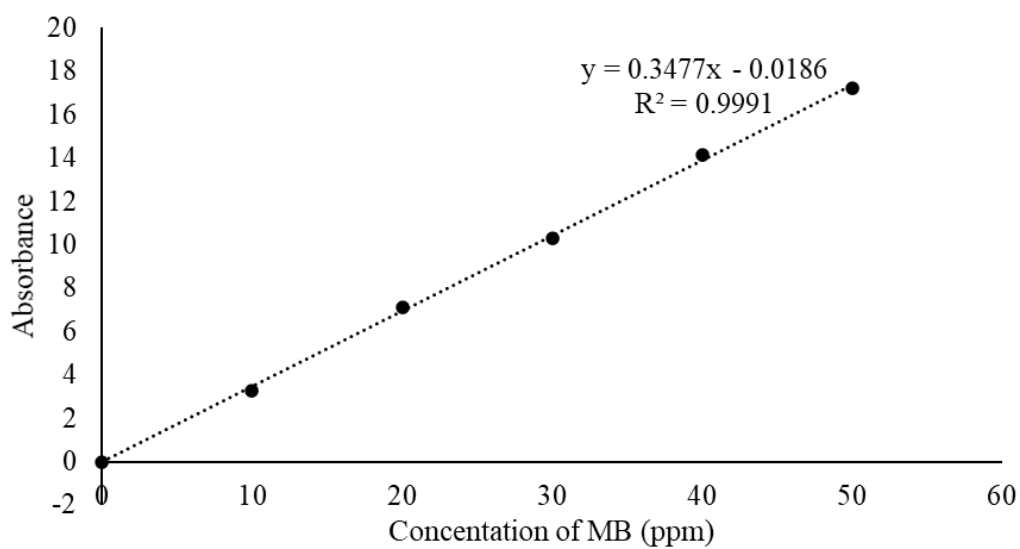
Figure D-2: Standard Calibration Curve for MB in Ethanol.

APPENDIX D: Calculation for Percentage of Adsorption and Degradation

To calculate the percentage of adsorption and degradation of MB, the concentration of MB after the adsorption and degradation process was first determined by using interpolation method. For example, by applying the UV-vis spectrophotometer, it can be found that the final absorbance of MB after the 5 h adsorption and degradation process was 0.0357. With the standard calibration curve in Figure C-1 (Appendix C), the final concentration of MB after the adsorption and degradation process can be computed as follow:

$$\frac{2.35 - 0}{10 \; ppm - 0 \; ppm} = \frac{0.0357 - 0}{C_{o,5 \; h} - 0 \; ppm}$$

$$C_{o,5 \; h} = 0.1519 \; ppm$$

The concentration of MB which was adsorbed and degraded can be calculated by deducting the final concentration of MB after 5 h from the initial MB concentration. Let's said the initial MB concentration was 50 ppm:

$$C_T = C_o - C_{o,5h}$$
$$= 50 \; ppm - 0.1519 \; ppm$$
$$= 49.8481 \; ppm$$

By mixing the collected MWCNTs-Fe$_3$O$_4$ nanocomposites with 20 mL ethanol solution and ultrasonicated for 30 min, the concentration of MB that was adsorbed will be determined again by using UV-vis spectrophotometer. For instance, the absorbance of MB that is adsorbed was found to be 4.118. Thus, the concentration of MB that was adsorbed can be calculated by interpolating the graph in Figure C-2 (Appendix C).

$$\frac{7.13 - 3.29}{20 \; ppm - 10 \; ppm} = \frac{4.118 - 3.29}{C_{adsorbed} - 10 \; ppm}$$

$$C_{adsorbed} = 12.1563 \; ppm$$

With the concentration of MB that was adsorbed, the concentration of MB that was degraded can be calculated.

$$C_{degraded} = C_T - C_{adsorbed}$$
$$= 49.8481 \ ppm - 12.1563 \ ppm$$
$$= 37.6918 \ ppm$$

Lastly, the percentage of adsorption and degradation of MB can be calculated as follow:

$$Percentage \ of \ Adsorption = \frac{C_{adsorbed}}{C_o} \times 100$$
$$= \frac{12.1563 \ ppm}{50 \ ppm} \times 100$$
$$= 24.31 \ \%$$

$$Percentage \ of \ Degradation = \frac{C_{degraded}}{C_o} \times 100$$
$$= \frac{37.6918 \ ppm}{50 \ ppm} \times 100$$
$$= 75.38 \ \%$$